The Thesis Committee for Ryan James Wagner
Certifies that this is the approved version of the following Thesis:

Investigation of the Correlation Between Waterflood Maturity and Appropriate Optimum Salinity

APPROVED BY
SUPERVISING COMMITTEE:

Quoc Nguyen, Supervisor

Maša Prodanović

Investigation of the Correlation Between Waterflood Maturity and Appropriate Optimum Salinity

by

Ryan James Wagner

Thesis

Presented to the Faculty of the Graduate School of

The University of Texas at Austin

in Partial Fulfillment

of the Requirements

for the Degree of

Master of Science in Engineering

The University of Texas at Austin

May 2020

Dedication

This work is dedicated to my family: to my father for instilling in me insatiable ambition; to my mother for her constant love and support; to my brother and sister, for their friendship and camaraderie; and to those lost along the way who impacted my life and this work.

Acknowledgements

First and foremost, I would like to acknowledge Dr. Quoc P. Nguyen, my supervisor. Dr. Nguyen stood by my side and continued to encourage me through numerous hurdles and hardships during my research and time at UT. Without his patience, belief in me, and mentorship, I would not have been able to complete this master's degree in Petroleum Engineering. I will always carry with me the desire to learn that Dr. Nguyen has instilled in me through his many lessons. Throughout my journey at the University of Texas at Austin, Dr. Nguyen has been an invaluable mentor, teacher, and friend.

Secondly, I would like to acknowledge Mr. Glen Baum, Mr. Gary Miscoe, and Mr. Daryl Nygaard for their support and knowledge pertaining to my experimental equipment. Without them, most of the experiments and research in the Hildebrand Department of Petroleum and Geosystems Engineering would not be possible.

I would also like to acknowledge Total USA for their support of this research.

Abstract

Investigation of the Correlation Between Waterflood Maturity and Appropriate Optimum Salinity

Ryan James Wagner, M.S.E.

The University of Texas at Austin, 2020

Supervisor: Quoc P. Nguyen

This work sets out to establish a correlation between waterflood maturity and the appropriate optimum salinity of a surfactant formulation. This is done by introduction of the novel concept of a critical waterflood "pre-flush," specifically its presence and effect on Low-Tension-Gas (LTG) injection. The conditions of this work are for an offshore process with high salinity, moderate permeability, and only seawater available for use during enhanced oil recovery (EOR).

LTG is a process that involves the co-injection of a surfactant solution and gas in order to achieve ultra-low interfacial tension from Type III microemulsion and mobility control due to generation of foam in the porous media. This technology has been used in various severe reservoir conditions such as high salinity, high temperature, and low permeability. Furthermore, field studies with similar injection strategy and use of foam have been conducted.

Phase behavior testing was first conducted to create and identify two surfactant formulations. These formulations would allow for the testing of different scenarios along

the research methodology outlined for this offshore project. Five coreflood experiments were then conducted to test these various scenarios. The pertinent data gained from the coreflood experiments were pressure drop during LTG, and oil cut, oil recovery, and effluent salinity of the LTG process.

The presence of a critical pre-flush and its effects on LTG were shown from the dataset gathered. It was determined that the salinity maturity of a waterflood and the resulting salinity environment for LTG was heavily impacted by the waterflood pre-flush. The impact of the pre-flush on the presence of foam and effectiveness of each coreflood is also analyzed. The existence of a correlation between the waterflood maturity and appropriate optimum salinity for EOR is shown in this work.

Table of Contents

List of Tables xi

List of Figures xii

Chapter 1: Introduction 1

1.1. Problem Statement 1

1.2. Research Objective 3

1.3. Methodology 3

Chapter 2: Background 5

2.1. Foam 5

2.1.1. Mechanisms of Foam Generation 5

2.1.1.1. Snap-Off 5

2.1.1.2. Lamella Division 6

2.1.1.3. Lamella Leave-Behind 7

2.1.2. Mechanisms of Foam Destruction 8

2.1.2.1 Film Drainage 8

2.1.2.2. Gas Diffusion 9

2.2. Microemulsion Phase Behavior 10

2.3. Low-Tension-Gas Injection 14

2.3.1. Laboratory Work 14

2.4. Field Studies Involving LTG or LTG Aspects 15

2.5. A New Design Concept of the LTG Process 16

Chapter 3: Experiment Materials, Equipment, and Procedure 18

3.1. Experiment Materials 18

3.1.1. Synthetic Brine 18
3.1.2. Crude Oil 19
3.1.3. Core Sample 19
3.2. Equipment 19
3.2.1. Core Holder 19
3.2.2. Mass Flow Controller 20
3.2.3. Liquid Pump 21
3.2.4. Back Pressure Regulators 21
3.2.5. Pressure Transducers 21
3.2.6. Effluent Collector 22
3.2.7. Oven 22
3.2.8. Accumulators 22
3.2.9. Valves 23
3.2.10. Coreflood Setup 23
3.3. Phase Behavior Experiment Procedure 25
3.4. Coreflood Experiment Procedure 25
Chapter 4: Results and Discussion 28
4.1. Phase Behavior Tests 28
4.2. Coreflood Experiments 31
4.2.1. Coreflood 1 32
4.2.2. Coreflood 2 40
4.2.3. Coreflood 3 45
4.2.4. Coreflood 4 50

4.2.5. Coreflood 5 55
4.2.6. Coreflood Summary 62
4.3. Pressure Drop 63
4.4. Apparent Viscosity 64
4.5. Oil Recovery 65
4.6. Oil Cut 66
4.7. Effluent Salinity 67
Chapter 5: Conclusion and Recommendations 70
5.1. Conclusion 70
5.2. Recommendations 71
References 72

List of Tables

Table 3.1: Synthetic seawater and formation water compositions (ppm TDS) 18

Table 3.2: Core Flood Experimental Properties 27

Table 3.3: Coreflood Injection Strategy 27

Table 4.1: Experimental and calculated results for corefloods 1 through 5 62

List of Figures

Figure 2.1: Progression of the snap-off foam generation mechanism (Ransohoff, 1988) 6

Figure 2.2: Progression of the lamella division foam generation mechanism (Ransohoff, 1988) 7

Figure 2.3: Progression of the lamella leave-behind foam generation mechanism (Ransohoff, 1988) 7

Figure 2.4: Pressure differential across curved surface in a foam lamella (Schramm, 1994) 9

Figure 2.5: Progression of microemulsion phase behavior with increasing salinity. "RF" in this figure is "recovery factor" (Sheng, 2015) 11

Figure 2.6: Plot of solubilization ratio vs. salinity, depicting Type I, Type III, and Type II microemulsion and the optimum salinity at the equal solubilization point. (Green and Willhite, 1998) 12

Figure 2.7: Plot of interfacial tension vs. salinity, depicting Type I, Type III, and Type II microemulsion and the optimum salinity at a point of equal interfacial tension. (Green and Willhite, 1998) 13

Figure 3.1: Schematic of similar coreholder type to that used in this work 20

Figure 3.2: A schematic of the coreflood experiment setup for each coreflood conducted in this study. "BPR" stands for backpressure regulator. "D," "S," and "FB/WF" represent the fluids contained in each piston accumulator: Drive solution, slug solution, and formation brine/waterflood. "MFC" stands for mass flow controller. "DI Pump" stands for deionized water pump. 24

Figure 4.1: Solubilization ratios with optimum solubilization of approximately 8.75mL/mL 29
Figure 4.2: Trend of increasing Type III salinity with increasing amount of alkyldiphenyloxide disulfonate. Ratio Defined as IOS:PO sulfate:IBA:alkyldiphenyloxide disulfonate 30
Figure 4.3: Solubilization ratios with optimum solubilization ratio of approximately 5.7 mL/mL 31
Figure 4.4: Permeabilities calculated for each section of the core, with a core-scale average permeability (CoreX) also calculated 32
Figure 4.5: Pressure drop profile of coreflood 1 oilflood 33
Figure 4.6: Pressure drop profile of coreflood 1 waterflood 34
Figure 4.7: Salinity and oil cut profile of coreflood 1 waterflood 35
Figure 4.8: LTG injection pressure drop profile compared to waterflood of coreflood 1 36
Figure 4.9: Apparent viscosity of coreflood 1 LTG injection 37
Figure 4.10: Core-scale LTG injection pressure drop profile compared to oil cut, oil recovery, and waterflood for coreflood 1 38
Figure 4.11: Alcohol injection pressure drop compared to LTG injection pressure drop profile of coreflood 1 39
Figure 4.12: Pressure drop profile of coreflood 2 waterflood 41
Figure 4.13: LTG injection pressure drop profile compared to waterflood of coreflood 2 42
Figure 4.14: Apparent viscosity profile of coreflood 2 LTG injection 43
Figure 4.15: Core-scale LTG injection pressure drop profile compared to oil cut, oil recovery, and waterflood for coreflood 2 44

Figure 4.16: Salinity, oil cut, and recovery profile of coreflood 2 LTG injection..... 45
Figure 4.17: Pressure drop profile of coreflood 3 waterflood of 0.433 pore volumes..... 46
Figure 4.18: LTG injection pressure drop profile compared to waterflood of coreflood 3 47
Figure 4.19: Apparent viscosity profile of coreflood 3 LTG injection 48
Figure 4.20: Core-scale LTG injection pressure drop profile compared to oil cut, oil recovery, and waterflood for coreflood 3 49
Figure 4.21: Salinity, oil cut, and recovery profile of coreflood 3 LTG injection with the Type III region of the High Salinity formulation shown in yellow box 50
Figure 4.22: Pressure drop profile of coreflood 4 waterflood of 0.4 pore volumes..... 51
Figure 4.23: LTG injection pressure drop profile compared to waterflood of coreflood 4 52
Figure 4.24: Apparent viscosity profile of coreflood 4 LTG injection 53
Figure 4.25: Salinity, oil cut, and recovery profile of coreflood 4 LTG injection with the Type III region of the Low Salinity formulation shown in yellow box. 53
Figure 4.26: Core-scale LTG injection pressure drop profile compared to oil cut, oil recovery, and waterflood for coreflood 4 54
Figure 4.27: Pressure drop profile of coreflood 5 waterflood of 0.4 pore volumes of formation water and additional 0.2 pore volumes of seawater 56
Figure 4.28: Absolute pressure profile of coreflood 5 waterflood of 0.4 pore volumes of formation water and additional 0.2 pore volumes of seawater. 57
Figure 4.29: Pressure drop profile of waterflood from each coreflood experiment..... 58
Figure 4.30: LTG injection pressure drop profile compared to waterflood of coreflood 5. 59

Figure 4.31: Apparent viscosity profile of coreflood 5 LTG injection. 60
Figure 4.32: Core-scale LTG injection pressure drop profile compared to oil cut, oil recovery, and waterflood for coreflood 5. 61
Figure 4.33: Salinity, oil cut, and recovery profile of coreflood 5 LTG injection with the Type III region of the Low Salinity formulation shown in yellow box. 62
Figure 4.34: LTG injection pressure drop profiles of all 5 corefloods..... 63
Figure 4.35: Apparent viscosity profiles of all 5 corefloods.. 64
Figure 4.36: Oil recovery profiles of all 5 corefloods.. 65
Figure 4.37: Oil cut profiles of all 5 corefloods..... 66
Figure 4.38: Effluent salinity profiles of all 5 corefloods 68
Figure 4.39: Effluent salinity profiles of all 5 corefloods beginning at the same datum . 69

CHAPTER 1: INTRODUCTION

1.1. Problem Statement

Offshore operations provide a unique characteristic for enhanced oil recovery (EOR), the endless availability of seawater for injection into the formation. This work considers the conditions of an offshore operation where all produced water is disposed of, leaving only seawater available for enhanced oil recovery processes. More specifically, this work also considers high salinity, approximately 150,000ppm total dissolved solids (TDS) and moderate temperature, 55˚C that will be waterflooded with seawater. With these field constraints, this operation would be a prime candidate for low-tension-gas injection (LTG).

Low-Tension-Gas injection (LTG) is a chemical enhanced oil recovery process that consists of two aspects: mobility control and ultra-low interfacial tension. These aspects are accomplished respectively by the formation of foam in the porous media in combination with the use of a surface-acting agent, or "surfactant" to create microemulsion. There are three types of microemulsion: Type I, Type II, and Type III. Each type can be achieved at varying salinity, with Type III being the desired microemulsion type for ultra-low interfacial tension in chemical EOR processes. With these two aspects, residual oil can be solubilized, mobilized, and recovered. The LTG process accomplishes this through co-injection of gas, in this case nitrogen, and a surfactant solution. The combination creates foam in-situ, which reduces the relative mobility, or ability, of the gas to propagate. This trapped gas forces the liquid surfactant solution into low permeable areas, where it encounters oil. The solubilization of the oil forms Type III microemulsion, which mobilizes the residual oil and forms an oil bank, which propagates through the core and is produced, followed by a surfactant foam bank. Both aspects of the LTG process are highly contingent on the salinity, or electrolyte concentration of the injection environment. The dependence

of microemulsion on salinity will be discussed in Chapter 2, but precise injection conditions must be present for a successful LTG process.

Regarding the surfactant solution, each surfactant solution may be based on different formulations that produce varying microemulsion types at certain salinities. The "optimum" salinity occurs at the salinity in which Type III microemulsion forms. One surfactant formulation may produce the desired Type III microemulsion at a low optimum salinity, and another may produce Type III microemulsion at a high optimum salinity. In this specific case of an offshore chemical EOR project, the low optimum salinity formulation is near seawater salinity, and the high optimum salinity formulation would be much higher than seawater, closer to the formation water salinity.

There are advantages and disadvantages at both ends of the spectrum. For a low optimum salinity formulation, the favorable aspects are that surfactant adsorption to the rock surface is lower, aqueous stability is easier to achieve at low salinity, and the pool of which to choose surfactants from is much larger. The drawback is that the entire salinity range above the low optimum salinity is in the undesirable Type II microemulsion zone, and surfactant adsorption would be high and aqueous stability would be challenged at these salinities. For a high optimum salinity formulation, the advantages are that the formulation would be aqueous stable at the high salinity, and thus any salinity lower than that. However, there is a more limited surfactant pool for generating formulations with high optimum salinity, adsorption is higher at high Type III optimum salinity, and oil and water solubilization at higher salinity is generally less than a lower optimum salinity formulation.

Regardless of the benefits and drawbacks of high or low optimum salinity formulations, the determining factor of which to use is the maturity of the waterflood. A "mature" waterflood refers to one in which the reservoir has been waterflooded to the residual oil saturation. This is common terminology and maturity is only limited to the

consideration of oil saturation. However, during any period of waterflooding, the formation is going through a significant change in salinity as the waterflood liquid displaces the resident formation brine. In this offshore case, waterflood would be with seawater, which has a drastically lower salinity than formation water, causing a severe change in salinity.

Although the duration of waterflood directly impacts the salinity in the formation, the LTG process can be designed accordingly. It is possible to apply LTG at any state of the waterflood, given that different options for higher and lower optimum salinity are available. If given an immature waterflood, this would result in a higher salinity environment where the high optimum salinity formulation would be required. If given an extremely mature waterflood, the low optimum salinity formulation would be used in the lower salinity environment. There exists a correlation between the maturity of the waterflood with respect to salinity and the appropriate optimum salinity. This work sets out to identify this correlation, and define a critical waterflood pre-flush needed to achieve the appropriate salinity environment from waterflood for a given surfactant formulation.

1.2. Research Objective

The key objective of this work is to establish a correlation between waterflood maturity pertaining to salinity and the appropriate optimum salinity.

1.3. Methodology

First, an extensive literature review was conducted consisting of the mechanisms of foam generation and destruction, microemulsion phase behavior, LTG technology, and the laboratory and field works that have been completed using LTG. From the problem statement, a series of experiments were conducted that would test the novel nature of this work.

Microemulsion phase behavior tests were conducted until a certain formulation was discovered to be effective with a particular crude oil sample. This formulation was further adapted to various salinity environments given the addition of another component. The success of these microemulsion phase behavior tests allowed for experiments to be conducted that followed the goal of this work.

Five corefloods were conducted to create and test different environments representative of varying waterflood maturities. The key variable in these experiments being the salinity of the formation, as oil saturation was essentially fixed, which will be described in detail further into the work. The results were analyzed extensively in order to develop a full understanding of the prevalent physics of these experiments.

Conclusions are drawn and recommendations for future work necessary to develop further understanding of this technology are outlined.

CHAPTER 2: BACKGROUND

2.1. Foam

Foam is defined as a dispersion of gas in a bulk liquid (Schramm, 1994). Foam in porous media has been long studied in order to understand the mechanisms of foam generation and destruction, foam mobility, and propagation of fluids in the presence of foam. Better understanding of these aspects has allowed for further laboratory investigation and field testing of enhanced oil recovery techniques involving foams. Foam is useful in enhanced oil recovery due to its mobility control effect for injected fluids.

2.1.1. Mechanisms of Foam Generation

There exist three fundamental mechanisms of foam generation in porous media: "snap-off", "lamella division", and lamella "leave-behind". Snap-off is predominantly believed to be the responsible mechanism for the generation of initial foam films, with subsequent foam formation attributed to lamella division and lamella leave-behind (Kovscek and Radke, 1994).

2.1.1.1. Snap-off

Roof (1970) was the first to identify and describe the snap-off mechanism when studying residual oil and the formation of oil globules in pores. For general foam generation in porous media, snap-off occurs downstream of constrictions, where gas travels through a pore throat entering into a wetting liquid-filled pore space. The invading gas bubble must have a capillary pressure that exceeds the capillary pressure of the liquid-filled pore, the capillary entry pressure. Upon this capillary pressure difference, the liquid is forced out and the exiting liquid essentially "pinches" off the entering gas, leaving a discontinuous non-wetting gas phase roughly the size of the pore body.

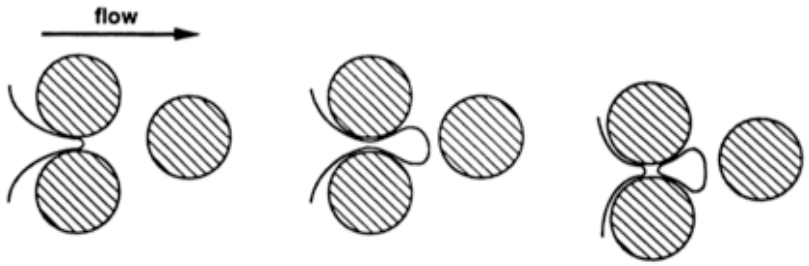

Figure 2.1: Progression of the snap-off foam generation mechanism (Ransohoff, 1988).

Snap-off has been identified as the dominant mechanism for foam generation of the three mechanisms, especially under co-injection conditions of surfactant and gas (Kovscek and Radke, 1994).

2.1.1.2. Lamella Division

Mast (1972) was the first to identify lamella division as a foam bubble generation mechanism. Lamella division occurs when a currently moving bubble encounters a point in which flow splits into two directions. If the foam bubble is larger than the pore body size, the bubble will divide into two and occupy both available paths; if smaller than the pore body size, the bubble will simply translate through one of the flow paths (Chambers, 1990). As mentioned, the foam bubble must not be stationary for this process to occur. If stationary trapped bubbles surround the adjacent pore bodies of the moving bubble, the occurrence of lamella division is much less likely due to the reduced number of available flow dividing points (Prieditis, 1988).

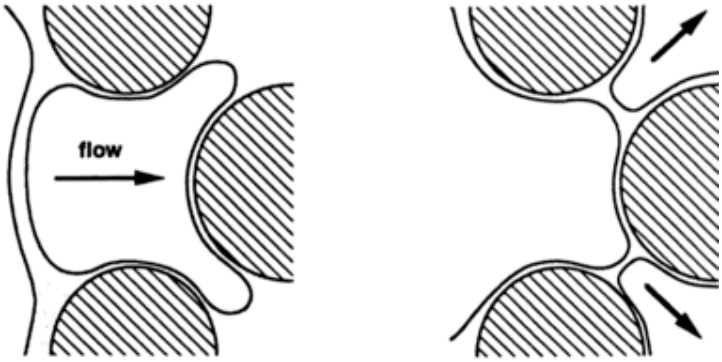

Figure 2.2: Progression of the lamella division foam generation mechanism (Ransohoff, 1988).

2.1.1.3. Lamella Leave-Behind

Lamella leave-behind occurs when two gas menisci travel through adjacent flow constrictions into liquid-filled pore bodies (Kovsckek and Radke, 1994). The menisci form a singular lens that is left behind and remains parallel to the flow direction (Owete and Brigham, 1987). This is the only foam propagation mechanism that forms parallel to the flow direction, instead of perpendicular to flow direction as in snap-off and lamella division. The leave-behind mechanism contributes to reduction of gas permeability, as it increases the amount of blocked flow paths to gas (Nguyen, 2000).

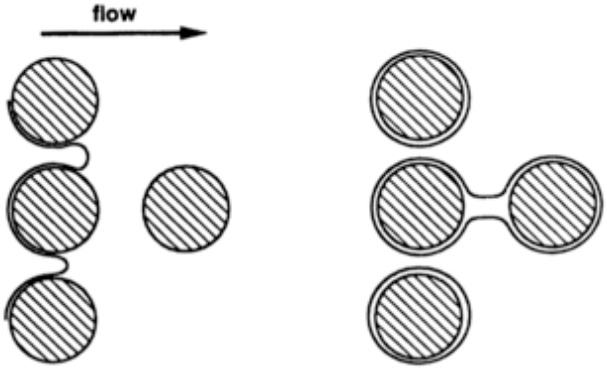

Figure 2.3: Progression of the lamella leave-behind foam generation mechanism (Ransohoff, 1988).

2.1.2. Mechanisms of Foam Destruction

Two mechanisms of foam destruction are widely discussed in literature regarding foam in porous media: Capillary-suction and gas diffusion (Kovscek and Radke, 1994). Nguyen (2000) discusses two more mechanisms of destruction: Liquid evaporation and condensation, and influence of additional phases. Liquid evaporation and condensation occur with the injection of dry gas and steam, respectively. The influence of additional phase flow regimes, such as two phase (water-gas), three phase (water-gas-oil), and four phase (water-gas-oil-surfactant) have varying effects on the destruction of foam in porous media. Many empirical and semi-empirical models have been developed to better understand the effect of additional phases. Marfoe *et al*. (1987) developed a two-phase model, expanded by Islam and Farouq Ali (1990) for effect of oil, which illustrates the generally negative effect of oil on foam.

2.1.2.1. Film Drainage

Capillary-suction is commonly regarded as the fundamental mechanism of foam destruction, as many works have found compelling evidence of this. Chambers and Radke (1991) and Jimenez and Radke (1989) are two works that support this notion. Lamallae film drainage is driven by gravity and laplace capillary suction (Nguyen, 2000).

Gravity drainage is when liquid travels through the generated lamellae network due to gravitational forces. Weaire (1997) discusses this concept further in their work, with forced drainage experiments. Capillary suction occurs at plateau borders in a foam lamellae. Schramm (1994) depicts the pressure differential across the curved surfaces in a foam lamella:

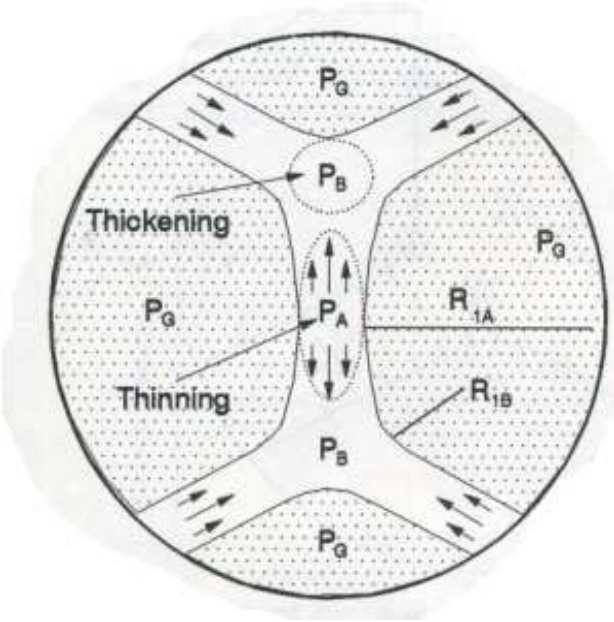

Figure 2.4: Pressure differential across curved surface in a foam lamella (Schramm, 1994).

The pressure at the center, P_A is larger than at the plateau border, P_B, causing liquid to be driven out of the lamella, resulting in bubble coalescence due to the disjoint pressure difference and capillary forces.

2.1.2.2. Gas Diffusion

Another mechanism of foam destruction is gas diffusion from smaller to larger bubbles. This mechanism is represented by the Young-Laplace equation, where gas on the concave section of a lamella is at a higher pressure than that at the convex side (Kovscek and Radke, 1994). The difference in the chemical potential results in gas diffusion and escape from the concave side to the convex side. This is most common in trapped gas bubbles, instead of translating bubbles. This process is more rapid in smaller bubbles (Bikerman, 1973).

2.2. Microemulsion Phase Behavior

Emulsions and microemulsions are dispersions of water-in-oil or oil-in-water. Emulsions are not thermodynamically stable, whereas microemulsions are. Emulsions, sometimes referred to as macroemulsions, have high interfacial tension and viscosity. Microemulsions have lower interfacial tension and viscosity. Microemulsions produced by surface-acting agents, also known as surfactants, are the key aspect of chemical enhanced oil recovery. The presence of microemulsion is dependent on the solubilization of oil and water, which at certain levels, can create ultra-low interfacial tension (IFT) environments, approximately 10^{-3} dynes/cm.

There are three fundamental types of microemulsions that are paramount for understanding chemical EOR processes, Winsor Type I, III, and II microemulsions. The sequence of these Winsor microemulsion types is listed as such because the system normally progresses from Type I to Type III to Type II. The progression of these Winsor microemulsion types is highly complex, and is dependent on brine salinity, temperature, surfactant concentration, surfactant type, brine composition, and the oil composition. Microemulsion systems can be understood by performing phase behavior experiments, where surfactant is added to an oil-brine system under varying salinity and temperatures. These three types represent the different microemulsions that can occur in an oil-brine-surfactant system, or microemulsion system.

In a Winsor Type I microemulsion, the surfactant forms an oil-in-water microemulsion in the aqueous phase. In a Winsor Type III microemulsion, microemulsion forms between the oil and water phases, creating a third phase in the presence of excess pure oil and pure water phases. This is the Winsor microemulsion type responsible for ultra-low interfacial tension in chemical enhanced oil recovery, due to the solubilization of

both oil and water. In a Winsor Type II microemulsion, the surfactant forms a microemulsion with the oil phase, leaving an excess water phase.

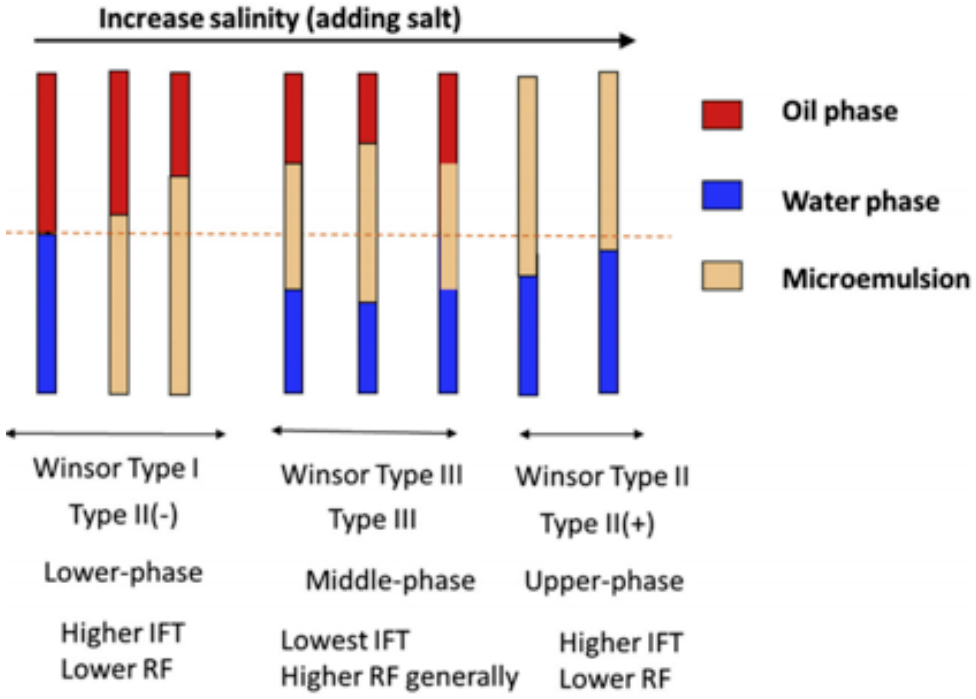

Figure 2.5: Progression of microemulsion phase behavior with increasing salinity. "RF" in this figure is "recovery factor" (Sheng, 2015).

The key result of microemulsion phase behavior experiments are the solubilization ratios of oil and water. They can be calculated using the following relationships:

$$Oil\ Solubilization\ Ratio = \frac{Volume\ of\ Oil\ in\ microemulsion}{Volume\ of\ surfactant\ in\ microemulsion} \quad \text{.....(2.1)}$$

$$Water\ Solubilization\ Ratio = \frac{Volume\ of\ Water\ in\ microemulsion}{Volume\ of\ surfactant\ in\ microemulsion} \quad \text{.....(2.2)}$$

Type III behavior occurs when both oil and water solubilization exist in the system. There exists an interface between both microemulsion and water and microemulsion and oil, with oppositely progressing interfacial tensions with increasing or decreasing salinity. The following figure demonstrates the progression of the Winsor types and the solubilization of oil and water with increasing salinity.

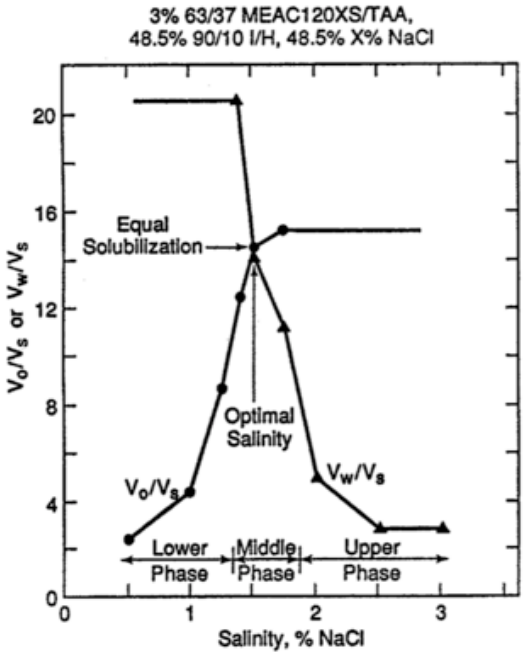

Figure 2.6: Plot of solubilization ratio vs. salinity, depicting Type I, Type III, and Type II microemulsion and the optimum salinity at the equal solubilization point. (Green and Willhite, 1998)

The optimum salinity, occurs where there is equal solubilization of both oil and water, at the point where interfacial tension of the water and oil interfaces are equal, despite their previously mentioned opposite progression. The Chun Huh correlation can then be used to relate the solubilization parameters of a microemulsion system to interfacial tension (Huh, 1979).

$$\sigma_{l3} = \frac{c}{R_{l3}^2} \quad \text{.....(2.3)}$$

Here, σ_{l3} is the interfacial tension between the excess oil or aqueous phase and the middle phase, R_{l3}^2 is the solubility ratio of oil or water by surfactant, and c is a constant with a typical value of 0.3. The interfacial tension of the previous solubilization ratio in Figure 2.6 is shown below in Figure 2.7.

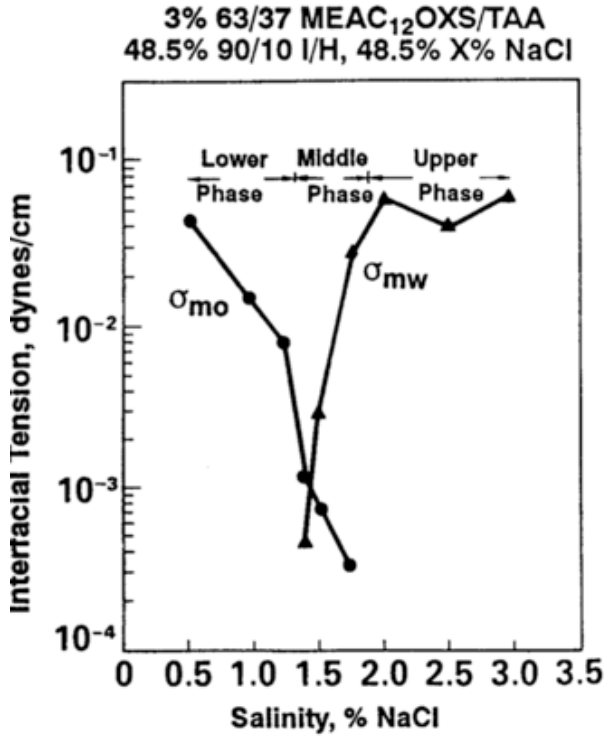

Figure 2.7: Plot of interfacial tension vs. salinity, depicting Type I, Type III, and Type II microemulsion and the optimum salinity at a point of equal interfacial tension. (Green and Willhite, 1998)

2.3. Low-Tension-Gas Injection

Low-tension-gas (LTG) injection is a relatively new technology that combines the technology of foam in porous media with surfactant-induced ultra-low oil-water interfacial tension. The LTG process consists of injection of a surfactant-gas solution to solubilize, mobilize, and displace residual crude oil after waterflood. Evaluation of LTG injection as a secondary process has also been conducted (Das, 2020). Similar to the Alkali-Surfactant-Polymer (ASP) process, ultra-low interfacial tension is achieved from surfactant injection for oil mobilization. However, mobility control is accomplished using foam instead of polymer. This allows the LTG process to be carried out in many different reservoir conditions.

2.3.1. Laboratory Work

The first proposed instance of utilization of foam in the oilfield was by Bond and Holbrook (1958). However, the concept of foam for mobility control was proposed by Lawson and Reisberg (1980) with their injection experiments of alternate slugs of gas and dilute surfactant. This work originally tested the concept at high temperature (90˚C), high permeability sandstone (~500mD), tight carbonate (9mD), and varying pressures. Expanding from this novel idea, LTG has been further studied experimentally for many different reservoir conditions for tertiary recovery. Szlendak (2012) showed to applicability of LTG to tight sandstone and carbonate (~10mD to gas). Nguyen *et al*. (2015) used LTG in high salinity, high temperature (85˚C) sandstone reservoir. Jong (2016) experimentally and theoretically investigated the LTG technology in high permeability (~500mD) sandstones to demonstrate the impact of salinity gradient on the low-tension-gas injection process. Das (2016) applied LTG in high salinity (>200,000ppm TDS), low permeability environment (2-20mD). Also, as mentioned, Das (2020) investigated and

evaluated LTG as a secondary recovery process, which proved to be technically feasible and economically attractive.

2.4. Field Studies Involving LTG or LTG Aspects

Many field studies stemming from the aforementioned foam origin works of Bond and Holbrook (1958) and Lawson and Reisberg (1980) have been completed that show mobility decrease of injected gas, increased sweep efficiency, and higher oil production. There exist various examples of successful foam injection field projects throughout recent history. Hirasaki *et al*. (1997) demonstrated the use of surfactant/foam injection in an aquifer remediation process at Hill Air Force Base in Utah. Foam was utilized to solubilize and mobilize a contaminant at the bottom of the aquifer by diverting the liquid into the low permeability zones of interest. Wang *et al*. (2001) details the first "ultra-low interfacial tension foam flood," where an alkaline-surfactant-polymer (ASP) foam (ASPF) was formed from the addition of natural gas to ASP fluid. The field test showed a volumetric sweep efficiency increase and an estimated final recovery of nearly 70% OOIP resulting from stable foam formation. Blaker *et al*. (2002) describes the success of a foam-assisted water alternating gas (FAWAG) project in the Snorre field on the Norwegian Continental Shelf in the North Sea. Large amounts of gas were stored and the GOR of the producing well was reduced, which was a major goal as the field was limited by its gas processing capacity. Sanders *et al*. (2012) evaluates the implementation of a CO_2 foam pilot study in the SACROC (Scurry Area Canyon Reef Operational Committee) Field in West Texas. The pilot showed that the foam could be generated and propagated under the reservoir conditions, as well as a 30% increase in oil production at an offset producing well. The learnings from these field studies and projects, coupled with laboratory and simulation

work, will combine to aid in the development of foam technology and implementation for enhanced oil recovery.

2.5. A New Design Concept of the LTG Process

This work investigates a design concept of the LTG process in moderately permeable (~100mD) carbonate rock, and high formation brine salinity (~150,000ppm TDS). However, the novel aspect of this work, which has yet to be investigated previously, is the application of waterflood as a "pre-flush" for the LTG process. A "pre-flush" is a certain pore volume injected of water used to accomplish two key aspects: mobile oil production and salinity alteration. A "mature" waterflood is normally used to describe a waterflood that has long-since broken through at the producing well. The maturity, in this sense, is regarding the production of the oil due to waterflood, and the remaining oil saturation. This work proposes the concept of waterflood maturity with respect to salinity.

It has been demonstrated experimentally that waterflood in a coreflood experiment can produce most of the mobile oil and decrease to very low oil cut production in as little as 0.4-0.5 pore volume of waterflood injected (Das, 2020). However, it may take over 2 pore volumes of seawater injection until the salinity of the formation is akin to the injected waterflood salinity, as seen in this study and previous works. Since microemulsion phase behavior, the key component of chemical EOR, is highly dependent on salinity; this creates the opportunity for exploration of this idea of waterflood salinity maturity. By ending the waterflood before the "mature" amount of pore volumes needed for full salinity transformation, exact "pre-flush" amounts of waterflood can be tested with the LTG process.

The volume of the waterflood "pre-flush" can be altered to cater to the optimum salinity of a certain surfactant formulation. On the other hand, optimum salinity and the

formulation could be altered to cater to a certain waterflood "pre-flush" volume, and thus a certain resultant in-situ salinity. Here, both reasonings are investigated to gain understanding on the presence of a "critical pre-flush." This is the size of the waterflood needed to provide not only the production of the majority of the mobile oil, but also sufficient salinity alteration that prepares the reservoir for the injected chemical solution in the LTG process. For example, a surfactant formulation with a high optimum salinity would require a smaller waterflood pre-flush than a surfactant formulation with a low optimum salinity. The number of pore volumes required to produce the mobile oil and alter the formation salinity to the high optimum salinity is less than required for the low optimum salinity. Economically, assuming both surfactant formulations were readily available, the high optimum salinity formulation with shorter waterflood (pre-flush) would be the correct choice for faster rate of return and more immediate cash flow. The novel idea of a correlation between waterflood maturity and the appropriate optimum salinity has not only a potential technical impact, but vast economic impact of projects in similar situations.

CHAPTER 3: EXPERIMENT MATERIALS, EQUIPMENT, AND PROCEDURE

3.1. Experiment Materials

3.1.1 Synthetic Brine

Synthetic seawater and formation water were prepared by mixing various components with deionized water. The compositions of the seawater and formation water were obtained from actual field samples. These liquids were used in phase behavior testing and in various injection stages in the coreflood experiments. Table 3.1 details the components of the seawater and formation water. It is important to note the relatively high divalent cation concentrations, indicated in the table.

Component	Seawater	Formation water
Na^+	14325	45112
K^+	451	1403
Ca^{2+}	**485**	**7255**
Mg^{2+}	**1367**	**3152**
Cl^-	27336	92842
TDS	**43965**	**149765**

Table 3.1: Synthetic seawater and formation water compositions (ppm TDS).

3.1.2. Crude Oil

The oil used in this study had a viscosity of 5.25 cP and density of 35.7 ˚API at the reservoir temperature of 55˚C. The oil was filtered down to 0.22 micron filter paper in order to remove any larger particulate that could contribute to plugging or flow issues upon coreflooding.

3.1.3. Core Sample

The core samples used were from an Estaillades Limestone outcrop block. The permeabilities and porosities tested resulted in approximate average values of 25% porosity and 100mD permeability, which are calculated during the coreflood experiment. The rock is water-wet. Core samples of 1" diameter and roughly 11.25" were drilled and used for the coreflood experiments.

3.2. Equipment

3.2.1. Core holder

The core holder is a 1" steel core holder made by Phoenix Instruments, capable of temperatures and pressures well beyond the purposes of this study at 55˚C and 1000psi backpressure. The core holder is made up of the external steel device, which has an open cylindrical cavity inside that is filled with a rubber sleeve, which also has a cylindrical cavity inside where the core will be positioned. The rubber sleeve has 3 pressure "taps" that extend from the core cavity to the outside of the steel core holder, where steel flow lines can be attached and connected to pressure transducers. The annular space between the rubber sleeve and the external steel core holder is filled with mechanical oil and pressurized with a hydraulic hand pump to a point 300-500psi above the internal core

pressure at all times. This ensures proper fluid injection through the core and safe containment of the pressures inside the core. The following schematic provided by Phoenix Instruments is provided to illustrate some of the aforementioned aspects of the core holder.

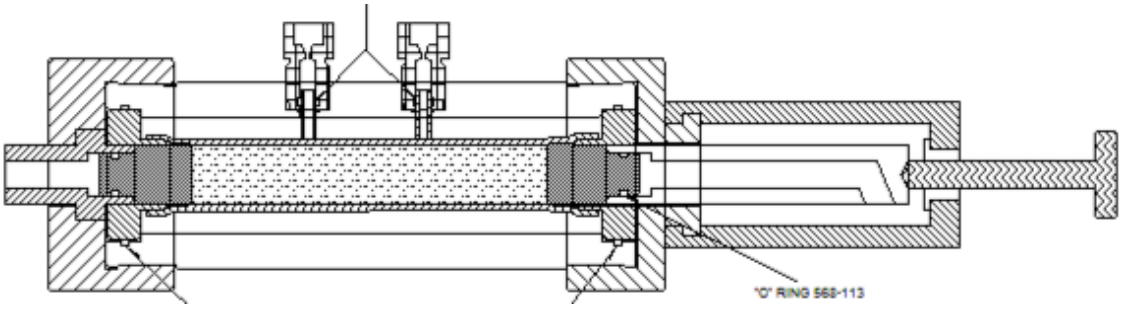

Figure 3.1: Schematic of similar coreholder type to that used in this work.

However, the particular core holder used in this study had three pressure taps, at 4", 6" and 8" from the bottom of the core. Only the 4" and 8" pressure taps are used, and the final one is capped for zero flow. The core is wrapped in heat-shrink plastic in order to protect the internal surface of the core holder rubber sleeve. The core is then drilled into to allow flow from the core into the pressure lines.

3.2.2 Mass Flow Controller

A Bronkhorst F-211CV-050-AAD-11-K type mass flow controller was used in these coreflood experiments to accurately inject N_2 gas into the system. The mass flow controller was factory calibrated and pressure tested. Calibration checks were done in the laboratory before implementing in the system.

3.2.3. Liquid Pump

A Chandler Engineering Quizix QX6000 was used for liquid injection. This precision pump used laboratory air to output deionized (DI) water, which pressurizes and expels desired experimental fluids from piston accumulators. The pump is checked for accuracy before each coreflood by injecting a specific amount of liquid into a container, which is then measured using a syringe repeater for accurate volume.

3.2.4. Back Pressure Regulators

Back pressure regulators are used in order to maintain the proper experimental pressure (reservoir pressure) on the core. Two back-pressure regulators are used at the core outlet to the effluent vials in order to mitigate any large fluctuations in pressure in the core due to the opening and closing of the BPR. This aids in mitigating the amount of noise in the data and allows for better resolution of the actual pressure behavior of the experiment.

A back pressure regulator is used on the confining oil as well in order to ensure that the confining pressure on the core does not exceed the 300-500psi pressure differential threshold outlined above. This is done to guarantee that the core does not experience a very large pressure differential, which is exceeding the strength of the rock, could cause pore collapse, permeability reduction, or other undesirable circumstances.

3.2.5. Pressure Transducers

Pressure transducers record the pressure at different points along the core. Two types were used: absolute pressure transducers and differential pressure transducers. The absolute pressure transducers record and read the pressure in that particular line segment, whereas differential pressure transducers record and read the difference in pressure between the two line segments connected. Three sections will be referred to in this work:

Section 1, Section 2, and Section 3. These sections represent different lengths along the core, with the pressure data determined by the differential transducers connected to each section. Section 1 represents the first 4 inches of the core from the inlet up, Section 2 represents the following 4 inches, and Section 3 represents the final ~3.125 inches of the ~11.125 inch core to the outlet.

3.2.6. Effluent Collector

The effluent collector is a device used to capture the effluent at various time intervals. This is useful in collecting exact fractions of a pore volume, which allows us to take "snapshots" of the liquid environment in the core at a particular pore volume injected.

3.2.7. Oven

An oven was used to house the core holder and accompanying lines in order to ensure that the experiment maintained a reservoir temperature of 55˚C at all times.

3.2.8. Accumulators

4 piston accumulators were used to displace 1. Formation brine/waterflood, 2. Crude oil, 3. Slug solution, and 4. Drive solution. The bottom of each accumulator is filled with deionized (DI) water below the piston, and above the piston lies the desired liquid. Deionized water from the liquid pump is injected into the appropriate accumulator in order to displace the desired liquid at an accurate rate.

3.2.9. Valves

Autoclave and Swagelok valves were used in this setup. Autoclave valves were mainly used due to their high temperature and pressure tolerance, making them suitable for in-oven use.

3.2.10. Coreflood Setup

A schematic of the coreflood experimental setup is shown below in Figure 3.2. All lines, accumulators, and transducers were thoroughly flushed with deionized water and evacuated of liquid and air before continuing with another coreflood. This was to ensure no contamination due to previously injected fluids.

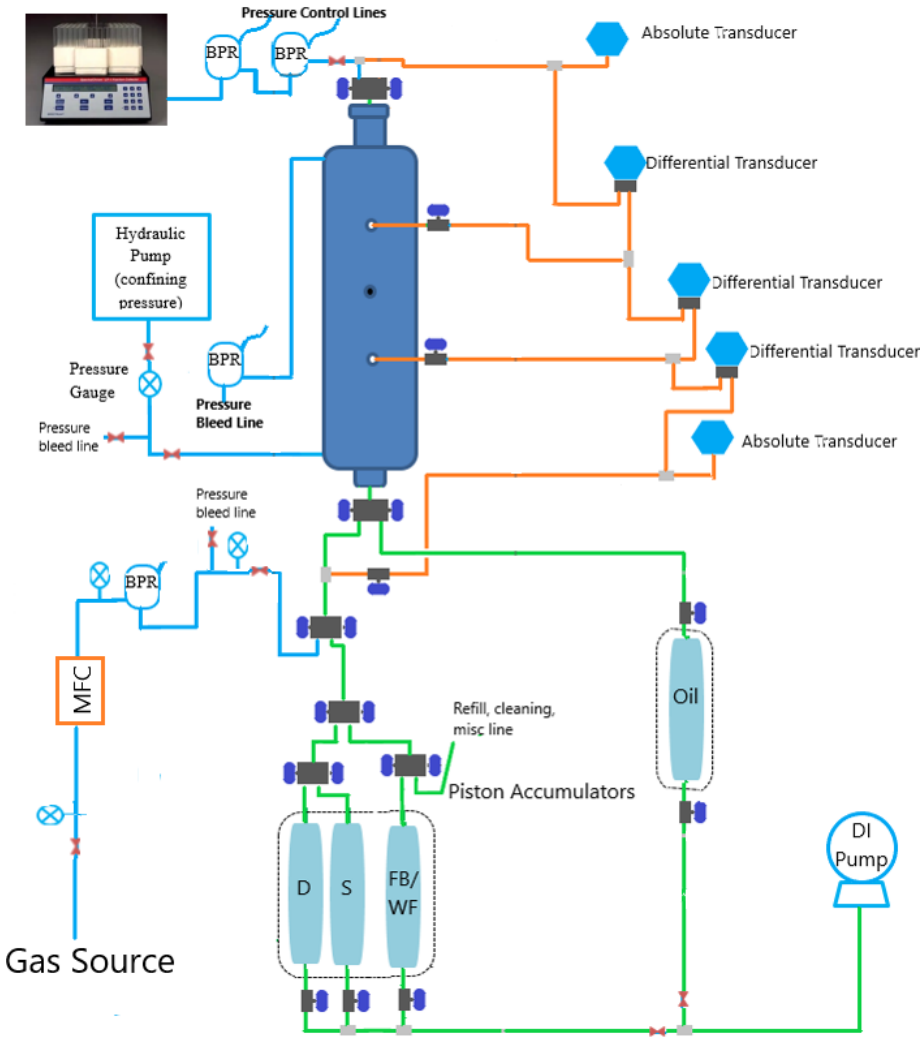

Figure 3.2: A schematic of the coreflood experiment setup for each coreflood conducted in this study. “BPR” stands for backpressure regulator. “D,” “S,” and “FB/WF” represent the fluids contained in each piston accumulator: Drive solution, slug solution, and formation brine/waterflood. “MFC” stands for mass flow controller. “DI Pump” stands for deionized water pump.

3.3. Phase Behavior Experiment Procedure

Both aqueous stability and microemulsion phase behavior tests were carried out in this work, as outlined in the research methodology. These tests are comprised of adding the surfactant solution to brine samples of increasing salinity to pipets and allowing them to reach equilibrium at the reservoir temperature, 55˚C. Aqueous stability tests are completed in the absence of oil, in order to observe the surfactant solution's aqueous stability at varying salinities by evaluating each sample for clarity, cloudiness, or phase separation. Once a formulation of acceptable aqueous stability is identified, crude oil is added in addition to the brine and surfactant solution. Microemulsion types can then be identified, which are dependent on the increasing salinity. The Type III microemulsion region and optimum salinity of each formulation are then identified.

3.4. Core Flood Experiment Procedure

A core sample 11.125 inches long and 1 inch in diameter are obtained from drilling Estaillades Limestone slabs. The cores are limited to this maximum length by the dimensions of the outcrop rock block. This size of core is also governed by the coreholder used. The cores were dried at 100˚C for over a week. The core holder is loaded into the oven, secured to the coreflood set-up flow lines, and the core is then checked for leaks at various pressures, until final leak testing at experimental pressure. The core is then vacuumed sufficiently to remove air from the system and prepare for the fluid injection phases. Several stages of fluid injections are carried out in the following sequence:

Brine saturation: Completely dry core is saturated with synthetic formation water (149,765ppm TDS, Table 3.1). Porosity and absolute permeability values were determined.

Oil Flood: The brine was then displaced by crude oil at various rate that aimed to achieve ~300 psi pressure drop across the core to encourage higher initial oil saturation.

This stage will continue until 100% oil cut is obtained in the effluent, ensuring as much brine has been displaced as possible. Oil relative permeability at residual water saturation was measured.

Waterflood: The oil was then displaced by synthetic seawater (43,965ppm TDS, Table 3.1). Seawater relative permeability at residual oil saturation was measured.

Low-Tension Gas (LTG) Injection: A surfactant slug of approximately 0.3 liquid pore volume (LPV) was co-injected with nitrogen gas at a fixed backpressure of 1000psig. The foam quality, or ratio of gas to liquid, was 50% (1:1) for all coreflood experiments. Slug solution salinity for all corefloods was equal to synthetic seawater salinity. The slug solutions used in the coreflood experiments were the Low Salinity and High Salinity formulations from the microemulsion phase behavior tests. Following the 0.3 liquid pore volume of slug solution, drive solution was also co-injected with nitrogen gas. Drive solution contained only one of the primary surfactants, 0.2 wt% Petrostep S2-HA. It was also co-injected with nitrogen gas at a fixed backpressure of 1000psig. This stage continued until no more oil is produced in the effluent. Drive solution salinity was also equal to ALS seawater salinity, 43,965ppm TDS. This injection strategy has been referred to as constant salinity, where slug and drive are at the same salinity.

Effluent samples were collected to evaluate oil recovery, oil cut, and salinity of produced water. Pressure drop across the core and core sections was recorded. The experimental properties used for all of the coreflood experiments can be found in Table 3.2. The injection parameters for each coreflood can be found in Table 3.3.

Rock Type	Limestone
Length	11.125 in.
Diameter	1 in.
Temperature	55˚C
Backpressure	1000psi
Waterflood Injection Rate	3 ft/D
LTG Injection Rate	3 ft/D (Liquid & Gas)
Gas Type	Nitrogen, N_2
Foam Quality	50%
Formation Water Salinity	149,765ppm TDS
Slug Injection Salinity	43,965ppm TDS (Seawater)
Slug size	0.3 PV
Slug Composition	Varied
Drive Composition	0.2 wt% IOS

Table 3.2: Core Flood Experimental Properties

Flood	Porosity (%)	Permeability (mD)	Objective	Formulation	Waterflood Type
1	20.52	97.74	Baseline	Low Salinity	Mature – Seawater
2	29.47	77.45	Baseline	Low Salinity	Mature – Formation Water
3	24.08	101.85	Pre-flush	High Salinity	0.4PV – Seawater
4	26.03	129.25	Pre-flush	Low Salinity	0.4PV – Seawater
5	26.24	95.20	Pre-flush	High Salinity	0.4PV – FW, 0.2PV - SW

Table 3.3: Coreflood Injection Strategy

CHAPTER 4: RESULTS AND DISCUSSION

4.1. Phase Behavior Tests

Aqueous stability and microemulsion phase behavior tests were conducted in this study to evaluate the success of each surfactant formulation. A successful formulation was created that consisted of IOS (Petrostep S2-HA), PO sulfate (Petrostep S13D), and isobutyl alcohol (IBA) in the ratio 1:1:1. The success criteria for this "main" formulation is that it generated Type III microemulsion at seawater salinity, a starting point for the evaluation of mature waterflood conditions during offshore processes. The components of this main formulation was used in all experiments, however, alkyldiphenyloxide disulfonate (Dowfax 2A1) was added to the other three components in ratio 1:1:1:0.4 to create a formula variation that produced different phase behavior results. The resulting formulation created Type III microemulsion at high salinity, which allows for the evaluation of LTG in immature waterflood salinity conditions during offshore processes.

With the main formulation, Type III microemulsion was observed from 43,965ppm TDS (seawater salinity) to approximately 50,000ppm TDS at 55˚C. The Type III optimum salinity for the main formulation was observed to be approximately 49,000ppm TDS. However, for the purpose of this study, seawater (43,965ppm TDS) was used as the injection salinity for all coreflood tests due to the replication of the aforementioned offshore conditions and injection strategy. The microemulsion phase behavior results are shown in Figure 4.1. In this figure, oil and water solubilization ratios are calculated in volume of liquid per volume of surfactant.

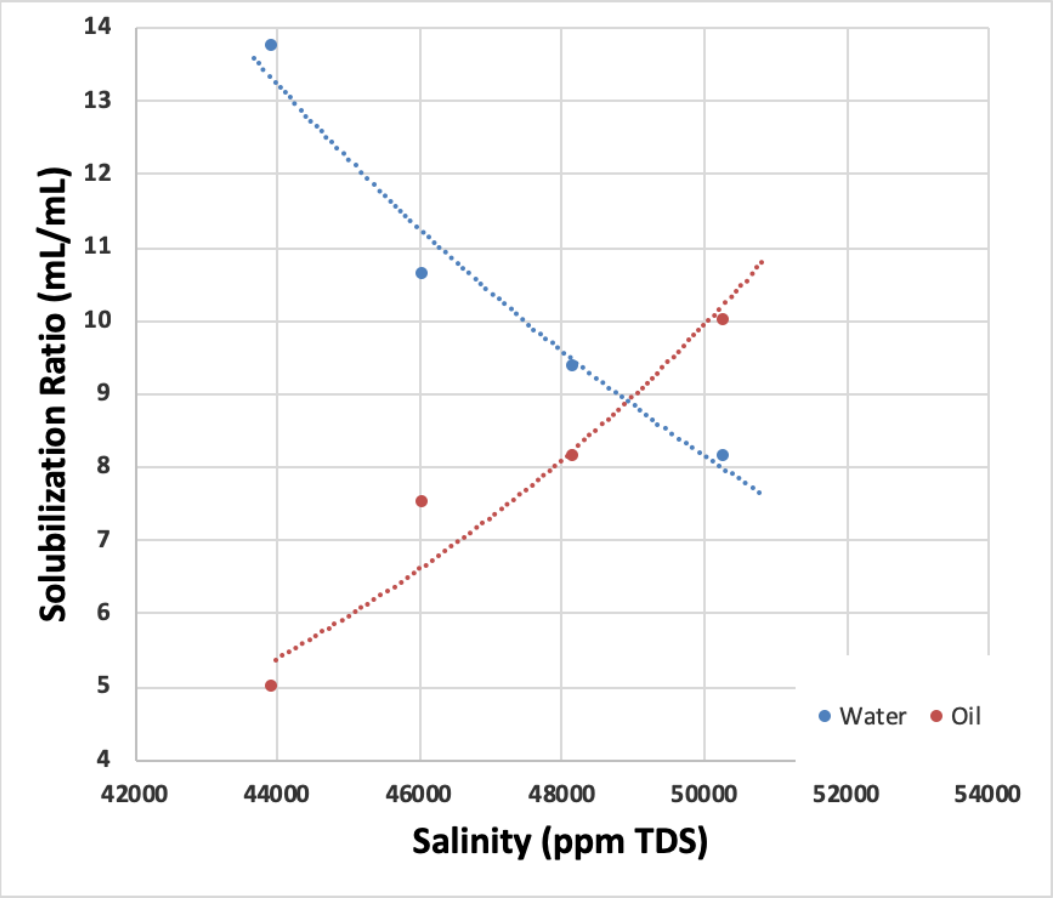

Figure 4.1: Solubilization ratios with optimum solubilization of approximately 8.75mL/mL.

By adding alkyldiphenyloxide disulfonate (Dowfax 2A1) to the main formulation in varying ratios, aqueous stability and Type III salinity were improved to higher salinities. As the Type III salinity increases, the window for Type III microemulsion widens, from approximately 5,000ppm TDS in the main formulation to approximately 15,000ppm TDS in the highest amount of alkyldiphenyloxide disulfonate. Figure 4.2 shows these trends, with ratios 1:1:1:0, 1:1:1:0.1, 1:1:1:0.2, and 1:1:1:0.4 of IOS, PO sulfate, IBA, and alkyldiphenyloxide disulfonate.

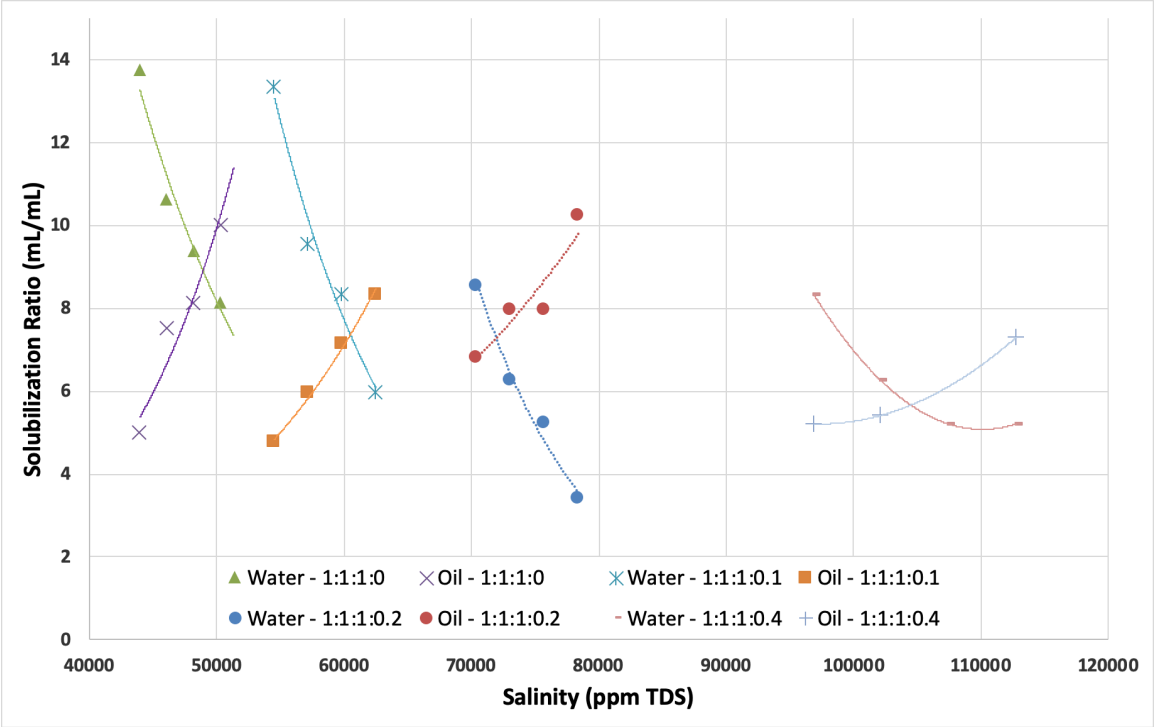

Figure 4.2: Trend of increasing Type III salinity with increasing amount of alkyldiphenyloxide disulfonate. Ratio Defined as IOS:PO sulfate:IBA:alkyldiphenyloxide disulfonate

In this study, only the main formulation and the formulation with alkyldiphenyloxide disulfonate ratio of 0.4 were used in the coreflood experiments. This is due to the experimental methodology to test the low salinity conditions of a mature seawater waterflood and the high salinity conditions of an immature seawater waterflood. These formulations will be hereby referred to as the Low Salinity formulation and the High Salinity formulation, respectively. This is due to their ability to create Type III microemulsion at low or high appropriate optimum salinity, respectively. With the High Salinity formulation (1:1:1:0.4 ratio), Type III microemulsion was observed from 97,000ppm TDS to 113,000ppm TDS at 55˚C. The Type III optimum salinity for the High

Salinity formulation was observed to be approximately 104,500ppm TDS. The microemulsion phase behavior results are shown in Figure 4.3.

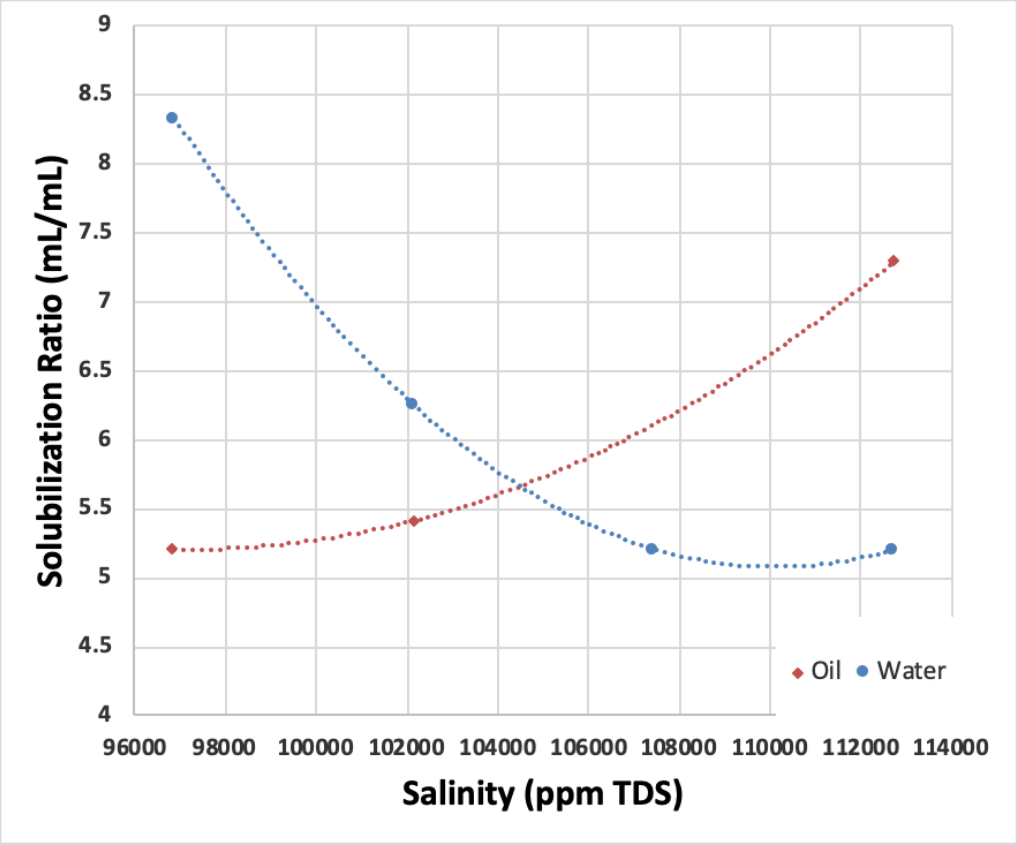

Figure 4.3: Solubilization ratios with optimum solubilization ratio of approximately 5.7 mL/mL.

4.2. Coreflood Experiments

These five coreflood experiments investigate the novel idea of waterflood maturity with respect to two parameters: salinity and oil saturation. Most of the mobile oil has been found to be displaced by approximately 0.4-0.5 pore volume of waterflood injected (Das, 2020). These experiments agree with that finding. However, the salinity environment at that point can be considered "immature", even though the oil saturation caused by

waterflood would be near residual oil saturation due to waterflood. These experiments investigate this difference and the effect on the successfulness of each experiment, but more importantly, the mixing occurring during these waterfloods, regarding the dual fronts of the water/oil front with dispersion affects in presence of oil, and waterflood/formation water front, in varying pore sizes. By injecting 0.4 pore volume waterflood in certain experiments, the salinity immaturity and impact on low-tension-gas injection can be investigated.

The result of each coreflood will be described in depth in the following sections. The first coreflood will be described in full detail from permeability testing to LTG injection in order to exhibit the entire discovery process undertaken for each coreflood. Then, all coreflood results will be compared and analyzed for key findings.

4.2.1. Coreflood 1

Coreflood 1 was conducted under appropriate optimum salinity conditions for the Low Salinity formulation. The objective of this coreflood was to test the LTG process under desirable conditions for the Low Salinity formulation. These conditions being after a waterflood that has achieved residual oil saturation to waterflood and a completely altered salinity environment from formation brine down to seawater. To begin, the core was saturated with brine and tested for permeability measurement to formation brine.

Permeability, mD					
Sec 1		Sec 2		Sec 3	
k1	104	k2	56	k3	148
CoreX					
k	97.74				

Figure 4.4: continued next page.

Figure 4.4: Permeabilities measured for each section of the core, with a core-scale average permeability (CoreX) also measured.

As seen in Figure 4.4, the core was seen to be moderately heterogeneous with respect to permeability. The core was then saturated with oil with the injection increasing in order to achieve nearly 300psi pressure drop to ensure high (greater than 50%) initial oil saturation. The following figure is the oil injection, and it is evident that the oil is moving through each section with the initial sectional pressure drop increases. The rate is increased further and the pressure rises to the pressure drop of interest.

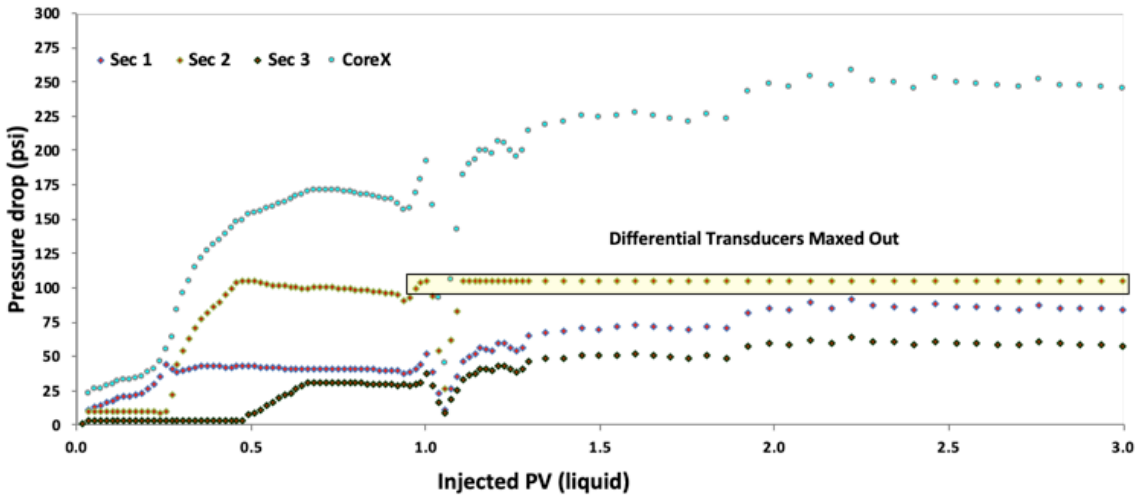

Figure 4.5: Pressure drop profile of coreflood 1 oilflood.

The core then underwent a waterflood of synthetic seawater (43,965ppm TDS) in order to achieve a residual oil saturation and salinity at synthetic seawater, which would be fully within the Type III window of the Low Salinity formulation. The waterflood pressure drop profile is shown in Figure 4.6.

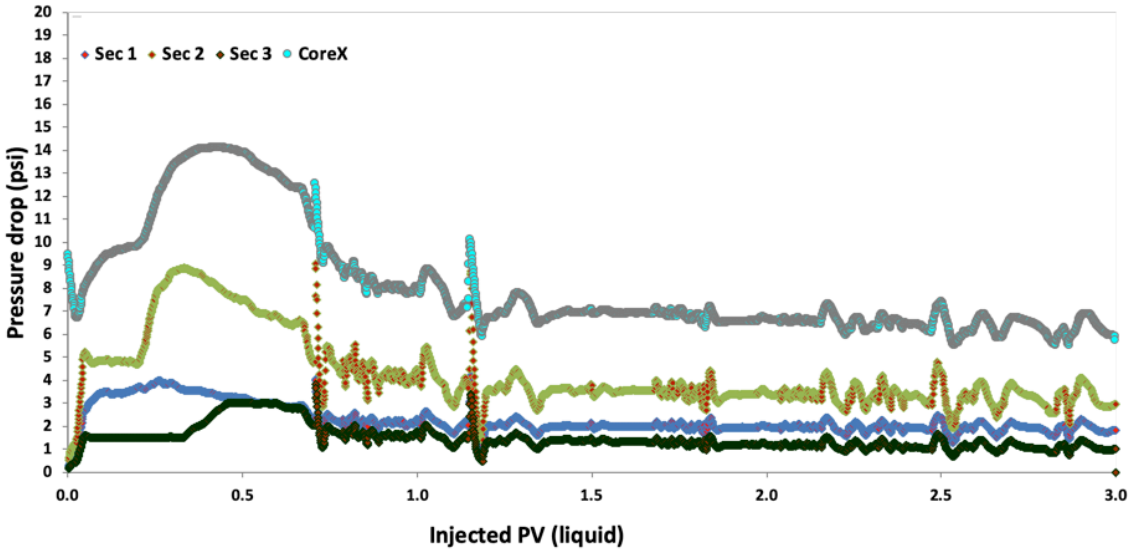

Figure 4.6: Pressure drop profile of coreflood 1 waterflood.

In order to ensure that the target salinity of synthetic seawater, 43,965ppm TDS has been achieved, effluent salinity measurements were taken during waterflood injection. It is also important to ensure that the core is at the true residual oil value, thus the effluent oil cut is monitored as well until 0% oil cut is reached. The oil saturation at the end of waterflood, S_{orw} is 22%, with the very low oil cut indicating that the mobile oil present in the formation was produced. The salinity and oil cut profiles are shown below in Figure 4.7.

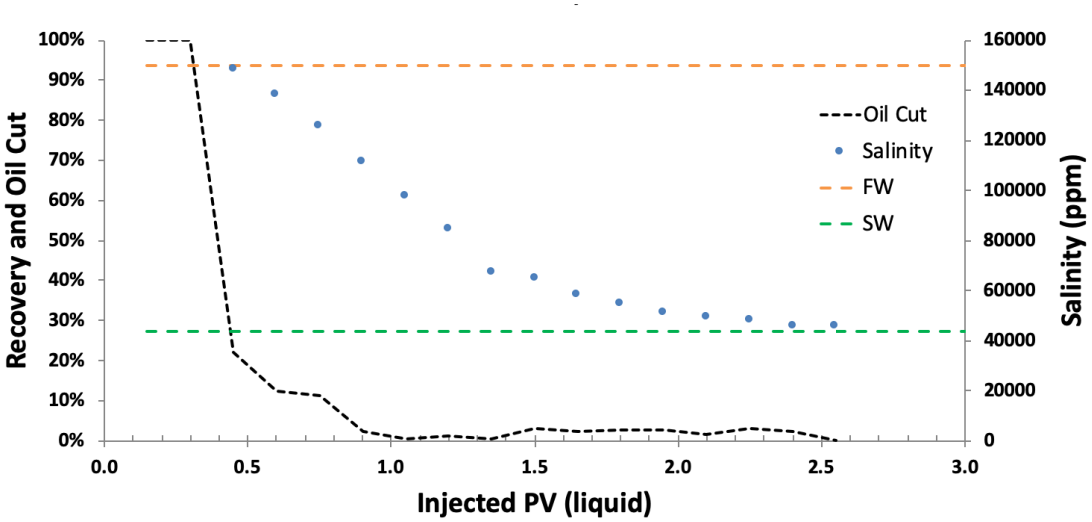

Figure 4.7: Salinity and oil cut profile of coreflood 1 waterflood.

Once the target salinity was reached and 0% oil cut was achieved, the LTG process could begin. The pressure drop profile is shown in Figure 4.8 and also depicts the waterflood pressure drop profile for comparison.

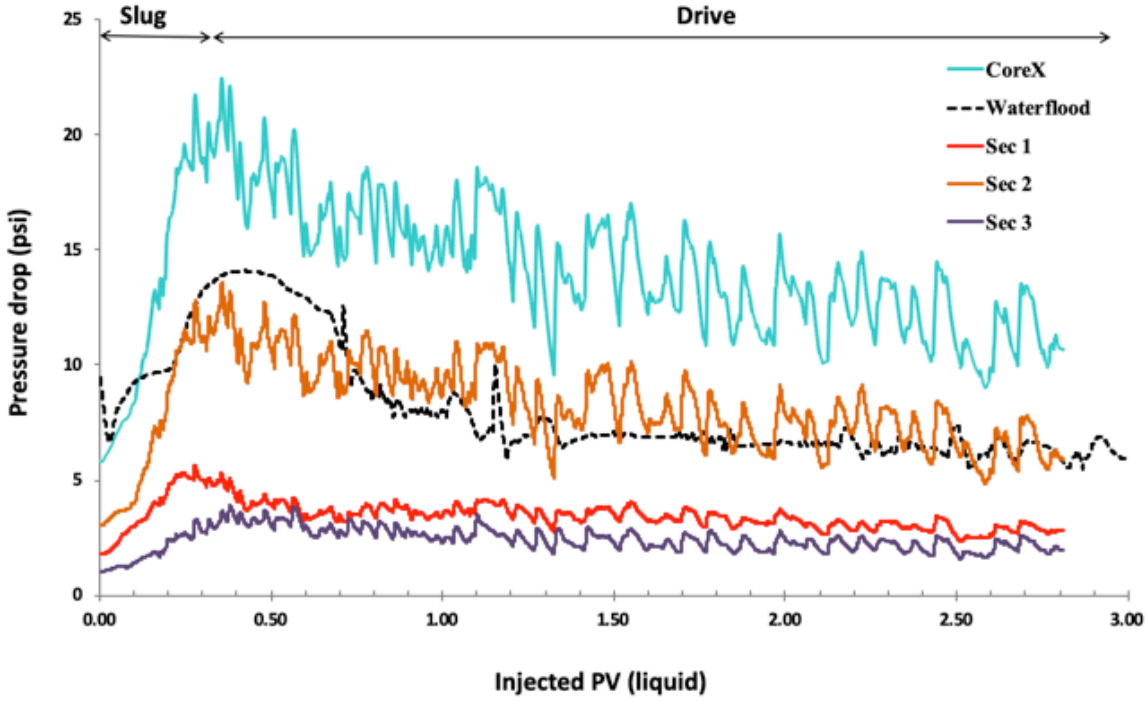

Figure 4.8: LTG injection pressure drop profile compared to waterflood of coreflood 1.

It is evident that the pressure drop across the core achieved a higher value than the waterflood pressure drop for the entirety of the LTG co-injection of the Low Salinity formulation and N_2. Increases in pressure drop in each section of the core can be seen from section 1, to section 2, and to section 3 as the oil bank propagates through the core. The degree of pressure increase in each core section is directly related to the permeability of each section. Section 2 had the lowest permeability and experiences the largest pressure drop increase, and vice versa for section 3. The apparent viscosity during the LTG process was calculated according to the measured permeability of each section and the appropriate core length of that section. The apparent viscosity during coreflood 1 is shown in Figure 4.9. This indicates better mobility control in the higher permeability zones (Veeningen et. al, 1997). Due to the trapped gas in the high permeability zones, surfactant-rich liquid is diverted into the low permeability zones, contacting the residual oil left from waterflood.

The apparent viscosity in each section is much higher during the formation and propagation of the oil bank than the viscosity of the crude oil, 5.25cP.

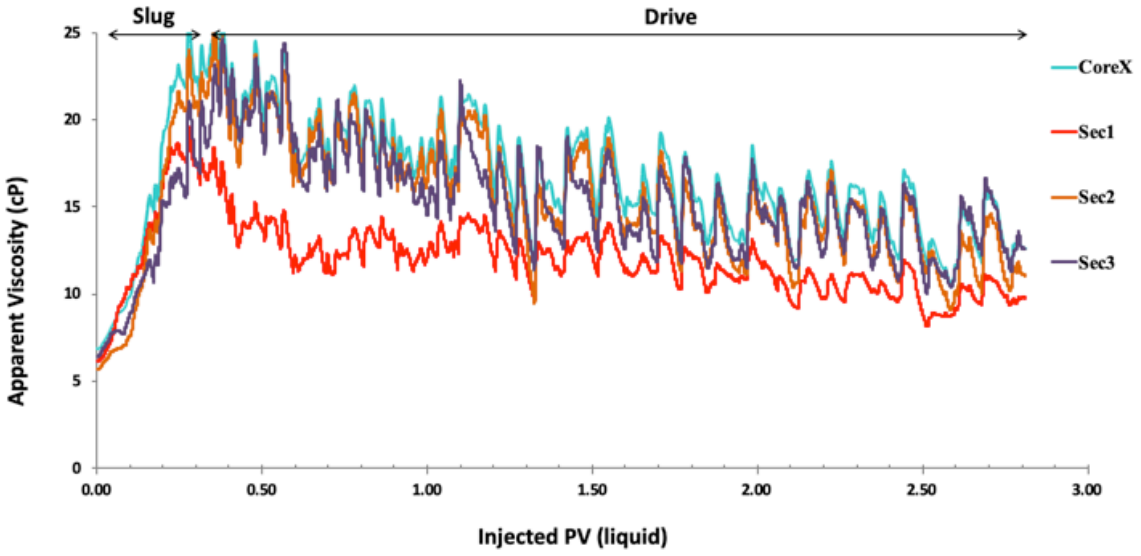

Figure 4.9: Apparent viscosity of coreflood 1 LTG injection.

The enhanced oil recovery for this coreflood was 75%, and a plot of the recovery, oil cut, and pressure drop profile is shown below in Figure 4.10.

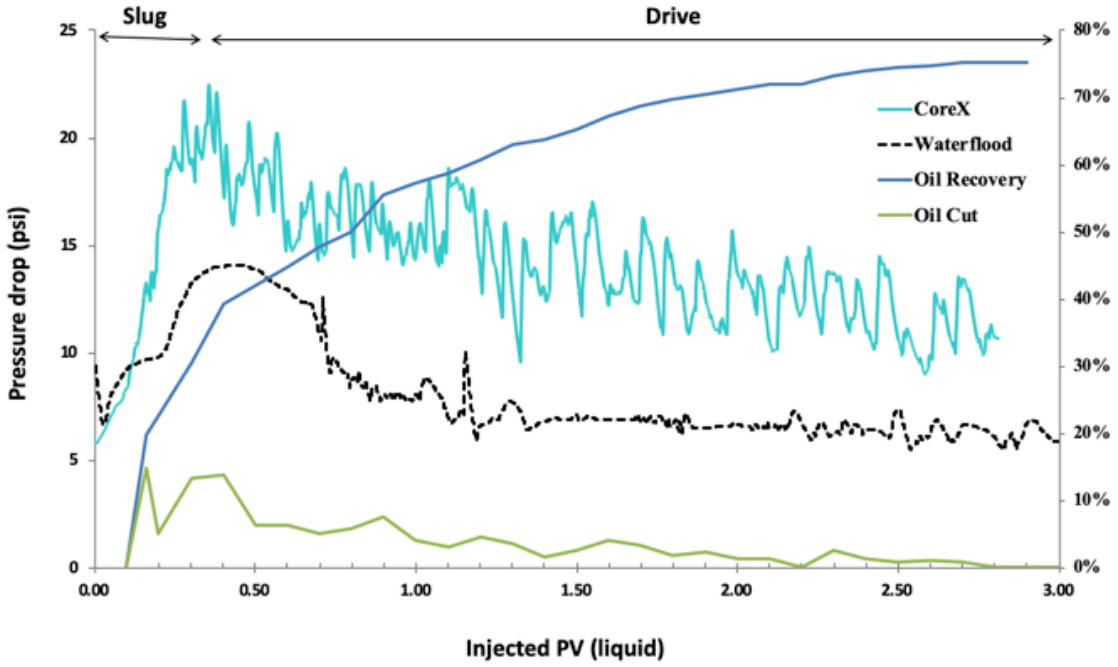

Figure 4.10: Core-scale LTG injection pressure drop profile compared to oil cut, oil recovery, and waterflood for coreflood 1.

This plot is useful for observing the progression of the oil bank caused by the LTG injection. The initial high oil cut and breakthrough of oil is observed at the initial pressure increase and the oil cut remains relatively high for approximately the following 0.3 pore volume. The pressure drop is also observed to decrease after the high oil cut period ends, showing that the oil bank has progressed through the core and been completely produced. Remaining oil not included in the bulk oil bank is slowly produced at low oil cut, as capillary number remains high due to the reduction of surface tension due to Type III microemulsion formation throughout the LTG process. Capillary number (N_{ca}) is defined as the viscous forces divided by the surface tension forces.

After the effluent oil cut is reduced to 0 for a period of time, the LTG injection ends. At this time, a brine solution containing approximately 25% ethyl alcohol is injected

into the core. This is done due to the alcohol's ability to coalesce the foam bubbles by breaking down the lamellae, releasing the trapped gas which compounds the effect of capillary suction and effectively "kills" the foam. The pressure drop decrease during this alcohol injection process from the roughly steady-state behavior at the end of the LTG process demonstrates the presence of foam. It is important to note that the flow rates of the liquid is equal to that of the LTG process, as well as the N_2, which continues to be injected to retain the two-phase injected flow regime. No oil is produced during the alcohol injection process. The alcohol injection data is shown below, where a linear line of best fit has been drawn on the alcohol injection data to show the increased rate of pressure drop decline compared to the LTG process. The pressure drop decreases to below the late-time waterflood pressure drop levels.

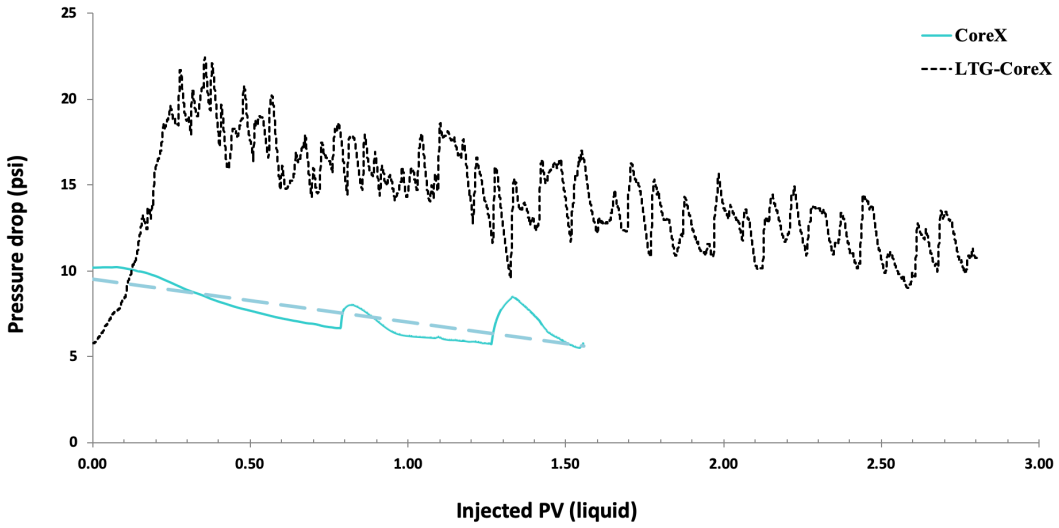

Figure 4.11: Alcohol injection pressure drop compared to LTG injection pressure drop profile of coreflood 1.

4.2.2. Coreflood 2

Given the success of coreflood 1 in the appropriate optimum salinity environment for LTG injection in the purely Type III microemulsion region, coreflood 2 was designed to test the same Low Salinity formulation in the most undesirable conditions. The LTG process was conducted after a formation water waterflood to the residual oil saturation due to waterflood. This environment is undesirable and suboptimal because it is completely in the Type II region (149,765ppm TDS), at a much higher salinity than the Type III region of the formulation (43,965 – 50,000ppm TDS). This was in order to understand the role of mobility control due to foam and ultralow IFT due to Type III microemulsion formation in such an environment with the direct comparison of the Low Salinity formulation's performance in corefloods 1 and 2. Like coreflood 1, coreflood 2 was also needed as a baseline of which to compare the performance of the next three corefloods to.

Coreflood 2 followed the same discovery procedure as coreflood 1. For coreflood 2 and the following corefloods, only the waterflood, LTG, and recovery data will be provided, as they will be the key points of discussion.

The waterflood data for coreflood 2 is seen below in Figure 4.12. In this coreflood, the core was waterflooded with pure synthetic formation water (149,765ppm TDS) in order to achieve the undesirable Type II environment, as discussed. The oil saturation at the end of waterflood, S_{orw} is 22%, with the very low oil cut indicating that the mobile oil present in the formation was produced.

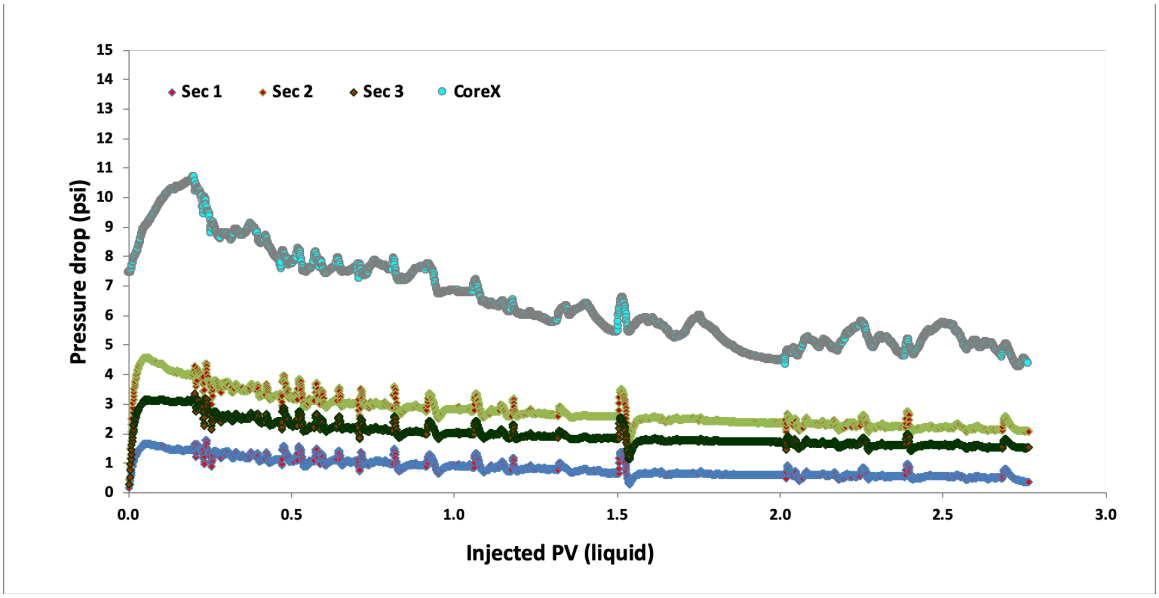

Figure 4.12: Pressure drop profile of coreflood 2 waterflood.

Once 0% oil cut was achieved in the effluent from waterflood, the LTG process could begin. The pressure drop profile is shown in Figure 4.13 and also depicts the waterflood pressure drop profile for comparison.

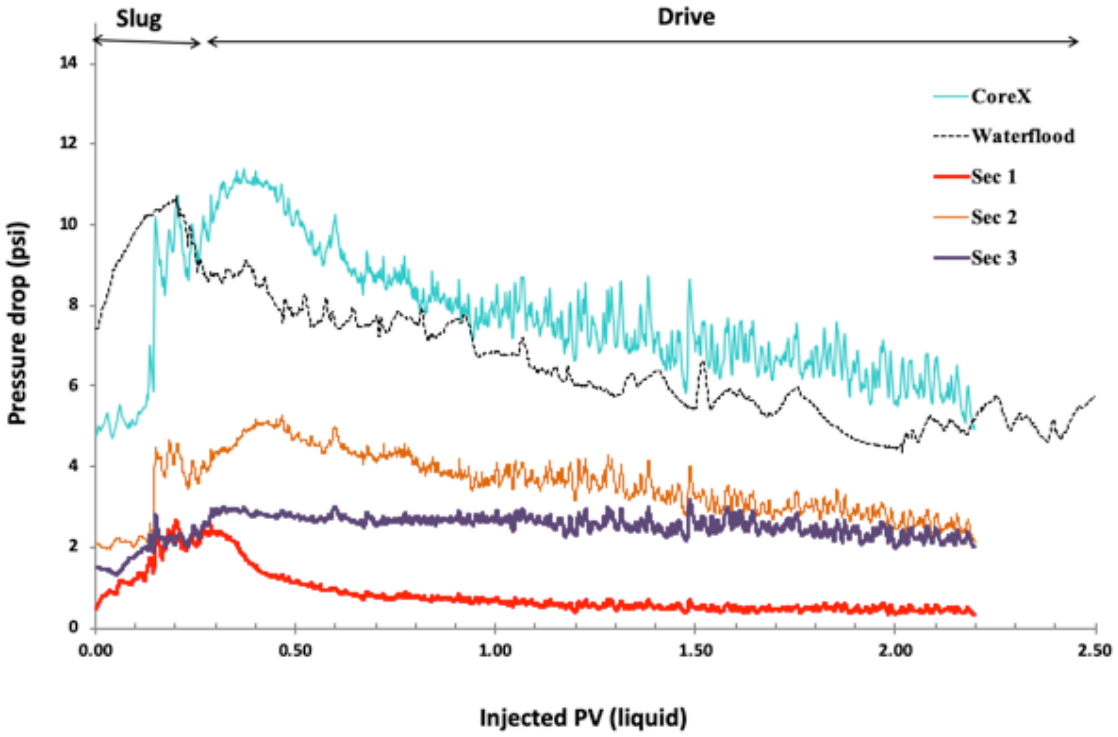

Figure 4.13: LTG injection pressure drop profile compared to waterflood of coreflood 2.

It is evident that the pressure drop across the core achieved a slightly higher value than the waterflood pressure drop for most of the LTG co-injection of the Low Salinity formulation and N_2. Increases in pressure drop in all sections of the core are less obvious in this case than coreflood 1. However, it appears that a sectional pressure drop increase and decrease occurred in sections 1 and 2, likely due to mobilization and production of a thin oil bank. This could also indicate the formation of foam in the early sections of the core, restricting flow and decreasing the relative mobility of the injected fluids, as seen in coreflood 1 for all three sections. After sections 1 and 2, the foam likely coalesced in the high salinity environment, failing to maintain mobility control throughout the entire flood, appearing to end at approximately 0.7 liquid pore volumes injected. The Low Salinity formulation could be robust enough to endure a certain degree of high salinity for a brief

period of time. This hypothesis is somewhat supported in the salinity data (Figure 4.16), where the slope of salinity decrease becomes less severe at approximately 0.7 liquid pore volumes injected, signaling less mobility control and increased dispersion.

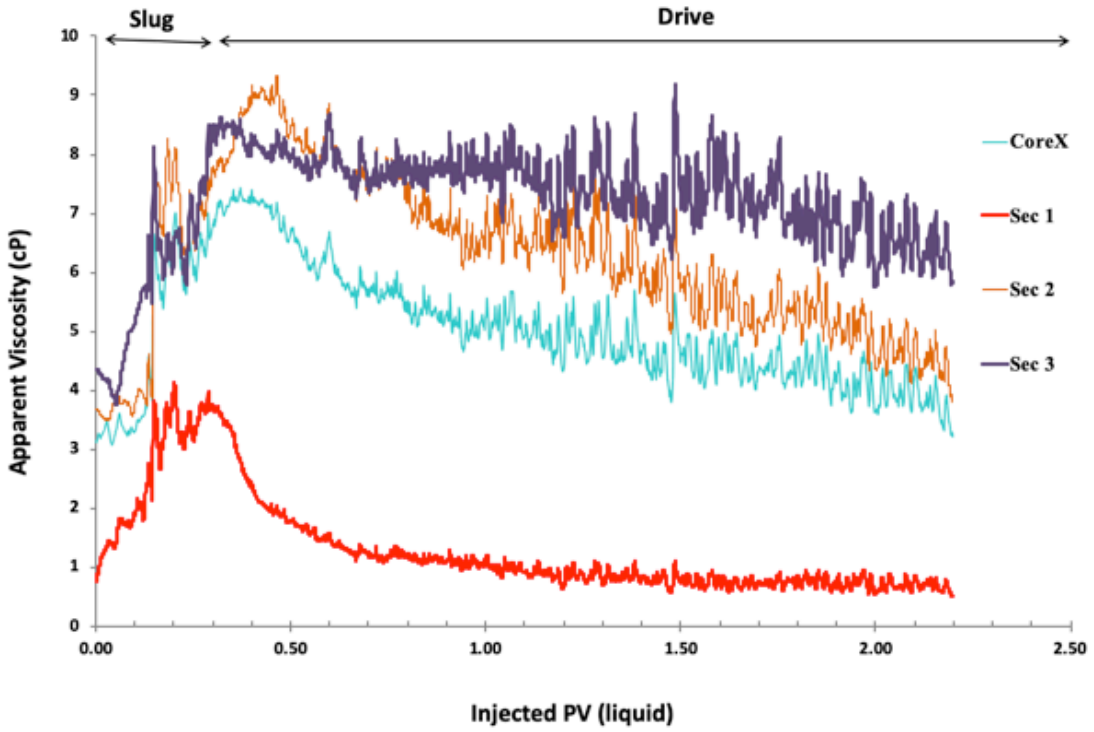

Figure 4.14: Apparent viscosity profile of coreflood 2 LTG injection.

Recovery of this coreflood was much lower than coreflood 1, resulting in 35% recovery, as seen in the plot of oil recovery, oil cut, and pressure drop profile shown in Figure 4.15.

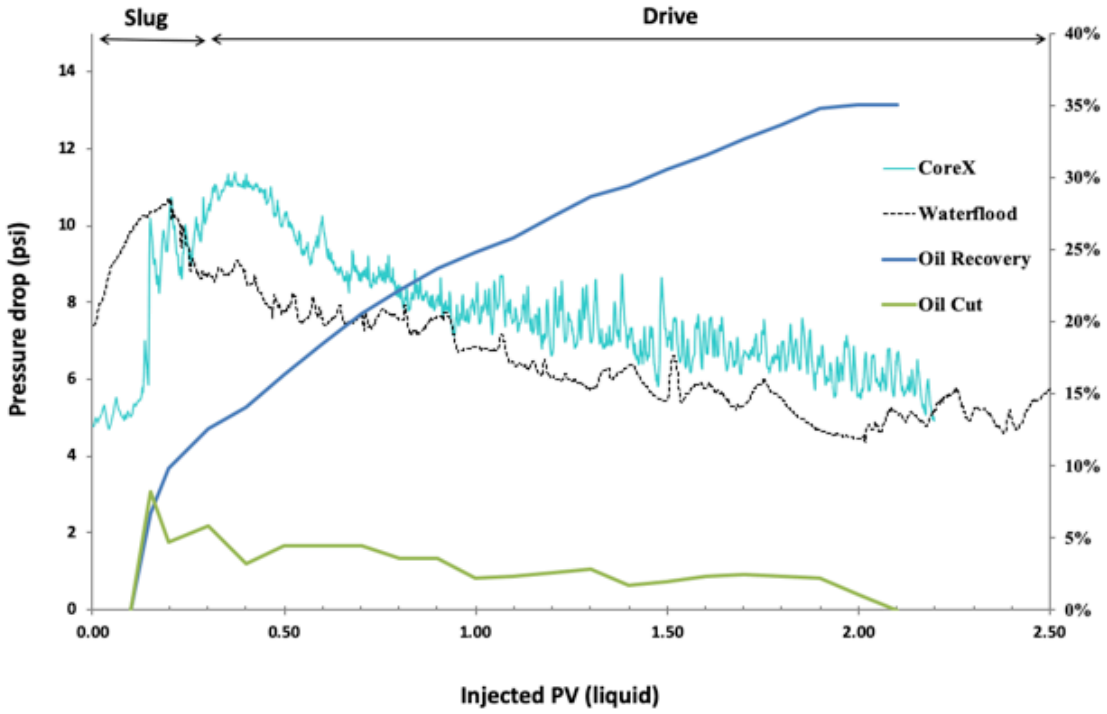

Figure 4.15: Core-scale LTG injection pressure drop profile compared to oil cut, oil recovery, and waterflood for coreflood 2.

As mentioned, solubilization of the oil in Type III microemulsion likely did not occur, which did not allow the formation of a large oil bank and mobilization of residual oil. The lack of Type III microemulsion can be further observed in the salinity data shown below in Figure 4.16, where the salinity of the core does not reach the Low Salinity formulation's optimum Type III region (43,965-50,000ppm TDS) until nearly 1.5 pore volume liquid injected. By that point, there was likely no available surfactant to solubilize oil as the 0.3 liquid pore volume of slug had long since been produced or adsorbed to the rock.

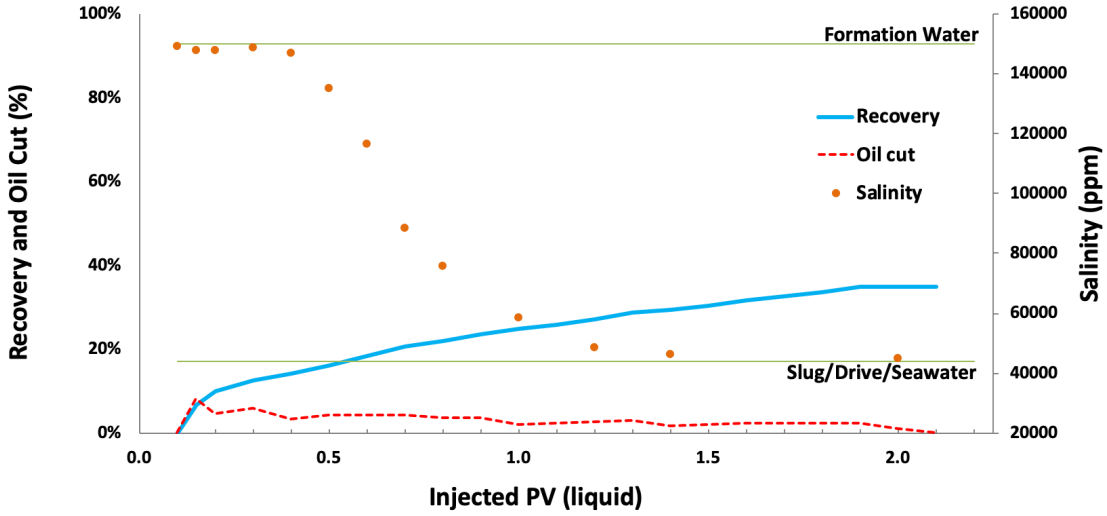

Figure 4.16: Salinity, oil cut, and recovery profile of coreflood 2 LTG injection.

Thus, without the aspect of ultra-low interfacial tension (IFT) of Type III microemulsion, the success of this coreflood relied solely on the presence of three phase flow. It appears that foam was generated, due to the relatively higher pressure drop when compared to waterflood. The observable sectional pressure drop increases in sections 1 and 2 is due to the mobile oil in a thin oil bank. This presence of foam diverted liquid into the low permeability zones and produced the residual oil left behind by the waterflood. The gas is the non-wetting phase, which occupies the larger pores, diverting liquid flow into the smaller pores and less permeable regions, as shown by Conn *et al*. (2014) and Nguyen *et al*. (2005).

4.2.3. Coreflood 3

Coreflood 3 was conducted under different conditions than corefloods 1 and 2, whereas only 0.4 pore volume of waterflood was employed, and the High Salinity formulation was used for LTG process. The motivation behind this coreflood was to

understand if an appropriate optimum Type III microemulsion salinity environment could be obtained by only using a smaller duration of waterflood before LTG. Das (2020) showed that most of the mobile oil is produced by 0.4-0.5 pore volume liquid injected during waterflood. Therefore, only the in-situ salinity continues to be altered past this amount of injection. Coupled with LTG injection, this coreflood would be taking place under appropriate optimum conditions of the High Salinity formulation, as long as the in-situ salinity is successfully altered with the 0.433 pore volume of seawater (43,965ppm TDS) injected before LTG.

As discussed, 0.433 pore volume of seawater waterflood was injected into the core to displace the mobile oil and begin to alter the salinity. The waterflood data is shown below in Figure 4.17.

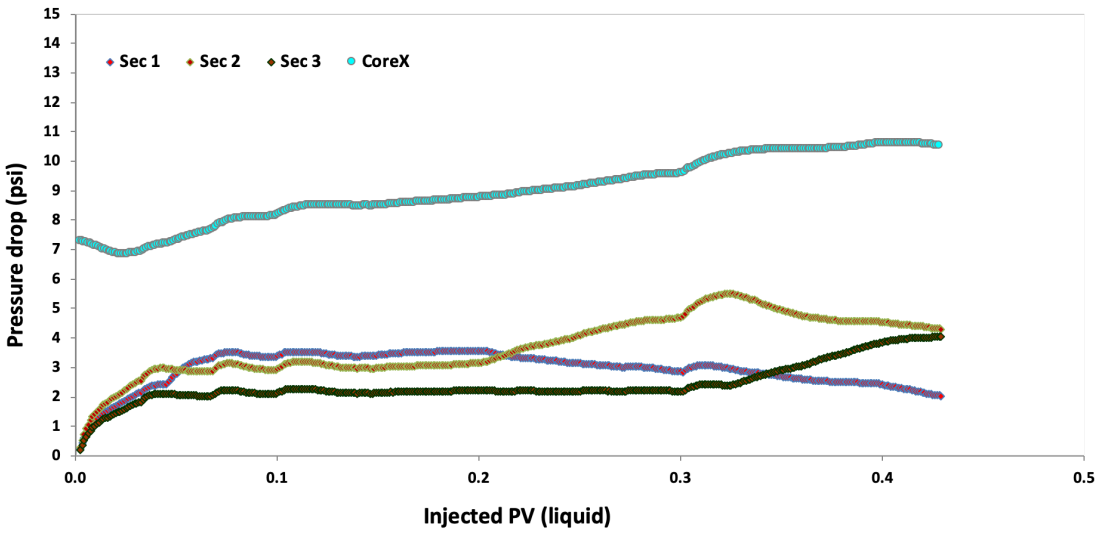

Figure 4.17: Pressure drop profile of coreflood 3 waterflood of 0.433 pore volumes.

The pressure drop profile clearly shows the oil moving through the core, as the pressure drop increases and decreases in sections 1 and 2, then reaches its peak in section

3 before the waterflood ended. This illustrates that the oil had been produced from the core into the outlet lines. The oil saturation at the end of waterflood, S_{orw} is 18%, with the very low oil cut indicating that this duration of waterflood was able to produce the mobile oil present in the formation.

The pressure drop profile of coreflood 3 is shown in Figure 4.18. Normally, after a long waterflood of multiple pore volumes, the late time pressure drop has decreased to its residual oil value. The LTG pressure drop would then increases from this point. However, due to the shortened waterflood duration, the pressure drop initially decreases because the waterflood ended before it achieved its late-time pressure drop value. This also causes the sectional pressure drop increases normally seen in an LTG flood to be harder to see, if observable at all. The apparent viscosity profile is shown further below in Figure 4.19.

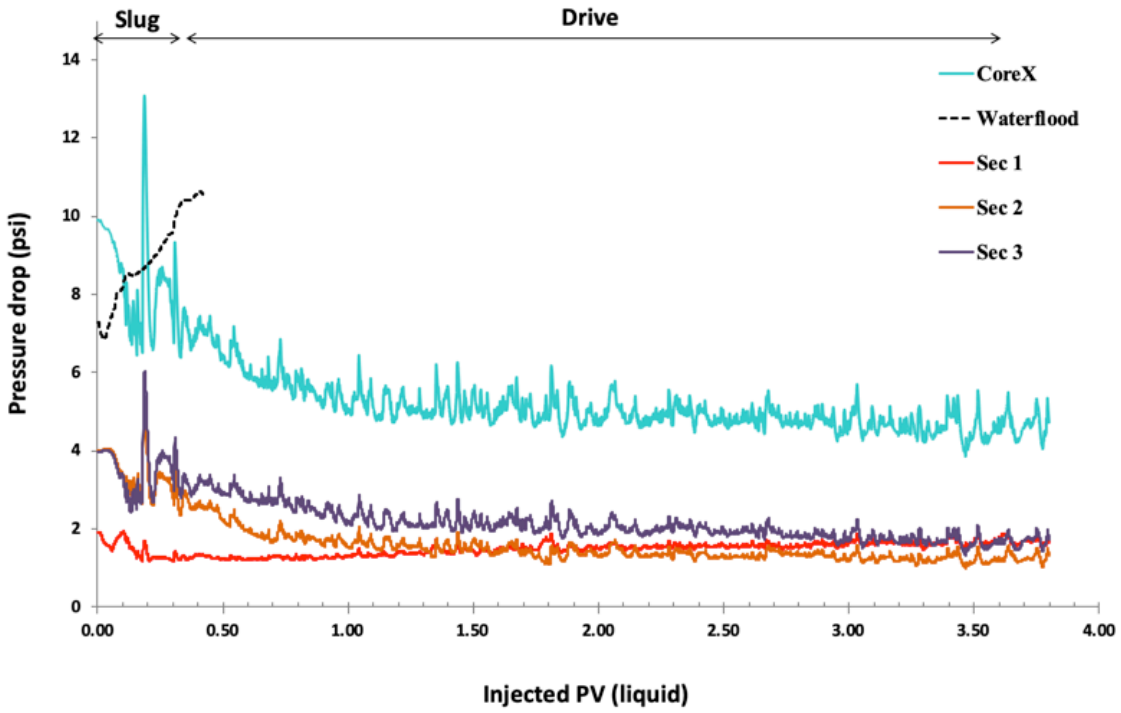

Figure 4.18: LTG injection pressure drop profile compared to waterflood of coreflood 3.

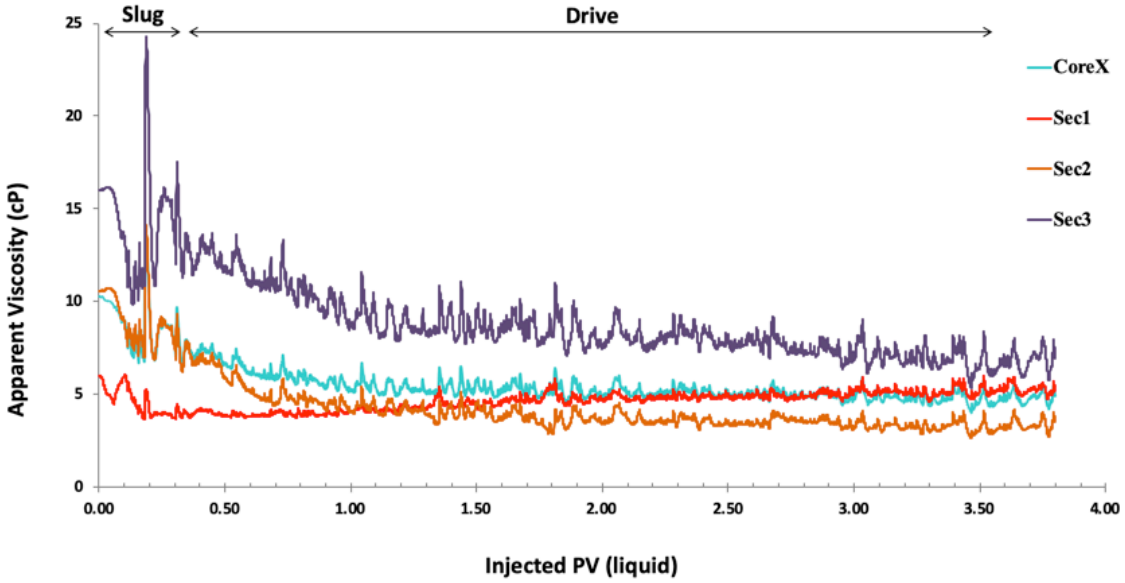

Figure 4.19: Apparent viscosity profile of coreflood 3 LTG injection.

Once again, the pressure drop profile compared to oil cut and recovery profile are shown in Figure 4.20. The initial oil cut seen in the plot represents the oil breakthrough from LTG, and is independent of the waterflood's production. The earlier waterflood oil was accounted for, but not represented in this plot. The division between waterflood and LTG oil recovery was identified by a reduction of the waterflood oil production and an obvious increase in the oil cut due to LTG.

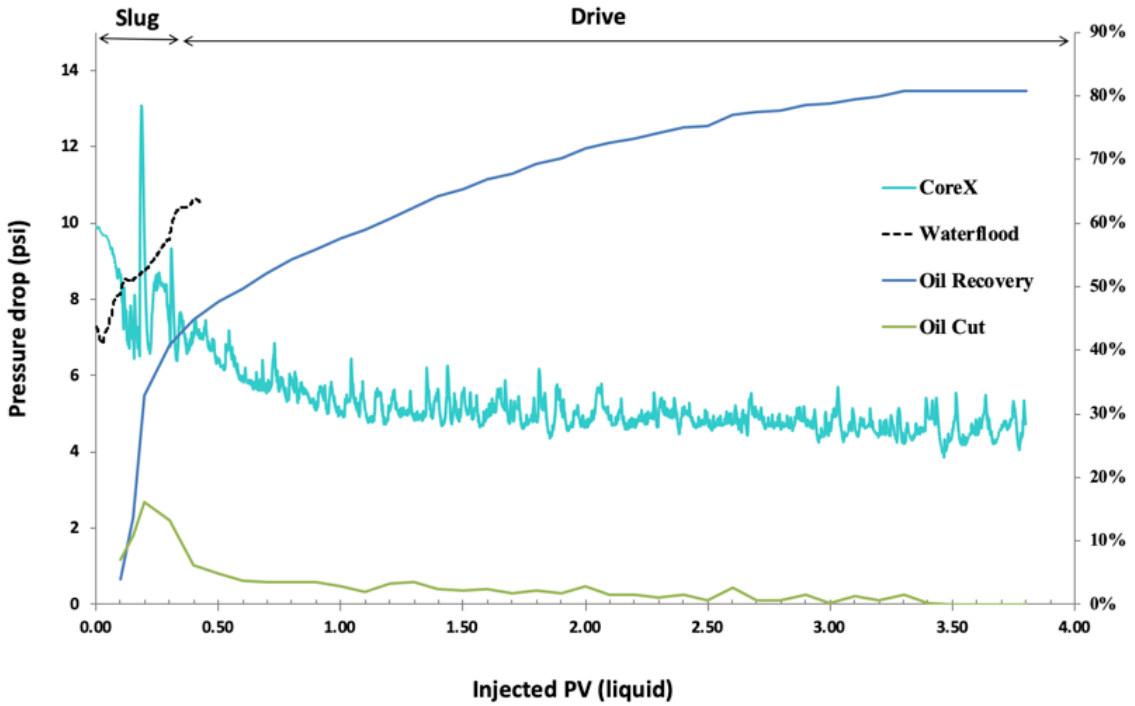

Figure 4.20: Core-scale LTG injection pressure drop profile compared to oil cut, oil recovery, and waterflood for coreflood 3.

It is evident that the LTG injection was successful in mobilizing and producing a substantial oil bank, given the increase in oil cut accompanied by a sharp pressure drop increase. The recovery of this coreflood was 81% of the residual oil, which is higher than coreflood 1 and considered very successful LTG recovery. The salinity data compared to the recovery profiles is shown below in Figure 4.21. The data clearly shows that the spike in oil cut and recovery is accompanied by effluent salinity directly within the Type III region of the High Salinity formulation (97,000 - 113,000ppm TDS).

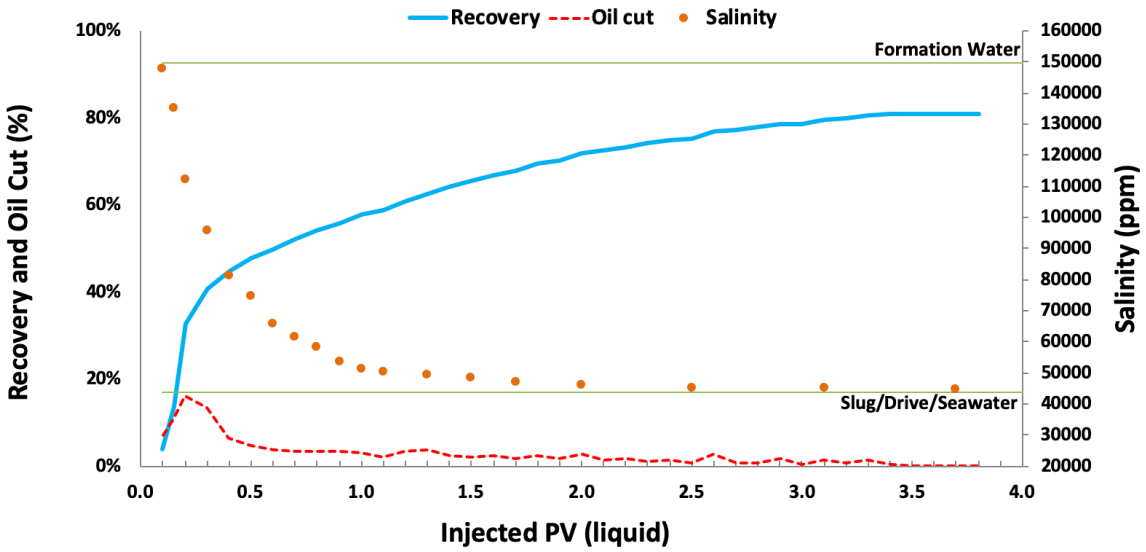

Figure 4.21: Salinity, oil cut, and recovery profile of coreflood 3 LTG injection with the Type III region of the High Salinity formulation shown in yellow box.

This plot illustrates that the 0.433 pore volume of seawater waterflood injected was successful in not only producing most of the mobile oil, but also in altering the salinity of the core and allowing the High Salinity formulation slug a favorable environment for Type III microemulsion formation. This supports that the critical pre-flush is near this value of 0.433 pore volumes seawater waterflood injected for the High Salinity formulation.

4.2.4. Coreflood 4

Next, a coreflood of the same conditions as coreflood 3 was completed with the Low Salinity formulation present in the LTG injection, instead of the High Salinity formulation. This was done in order to compare the effect of the Type III behavior on a coreflood with immature waterflood salinity mixing, as achieved in coreflood 3 by the 0.433 pore volume of seawater injected. The hypothesis being that coreflood 4 would achieve less recovery than coreflood 3 due to the less favorable salinity environment for

Type III microemulsion with the Low Salinity formulation. However, this coreflood was conducted to better understand the salinity mixing of the initial injection of the 0.4 pore volume of seawater and how that fluid front propagates.

The waterflood pressure drop profile is shown in Figure 4.22. This coreflood exhibits similar pressure drop plateau at 0.4 pore volume injected, which is similar in the other corefloods. The section 3 pressure drop begins increasing at 0.3 pore volume injected, and plateaus at approximately 0.4 pore volume injected, indicating that the oil bank has moved through this section and has been produced out of the core. The oil saturation at the end of waterflood, S_{orw} is 28%, with the very low oil cut supporting that this duration of waterflood was able to produce the mobile oil present in the formation.

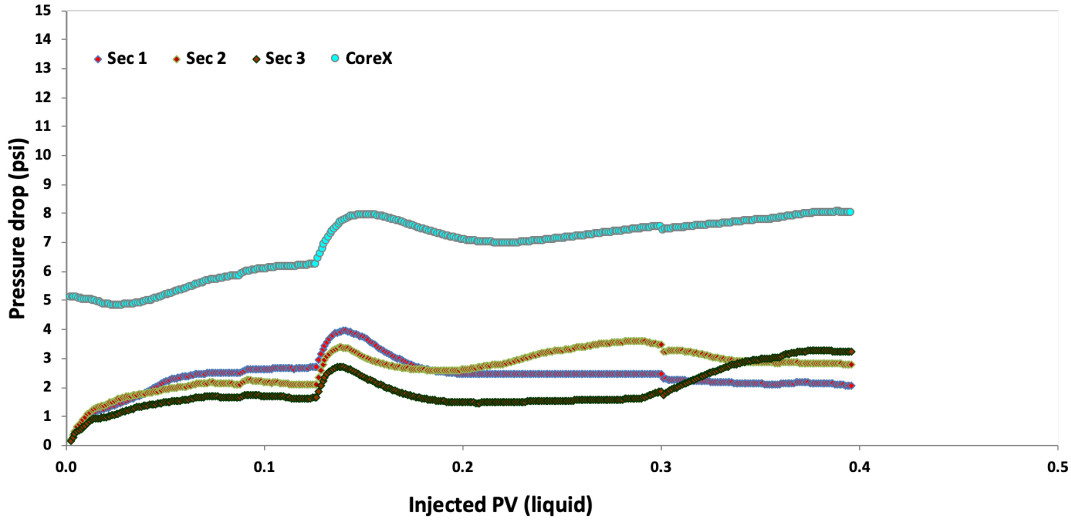

Figure 4.22: Pressure drop profile of coreflood 4 waterflood of 0.4 pore volumes.

The LTG pressure drop profile is shown in Figure 4.23 and clearly depicts the pressure drop due to LTG rising to nearly double the waterflood's peak pressure drop value.

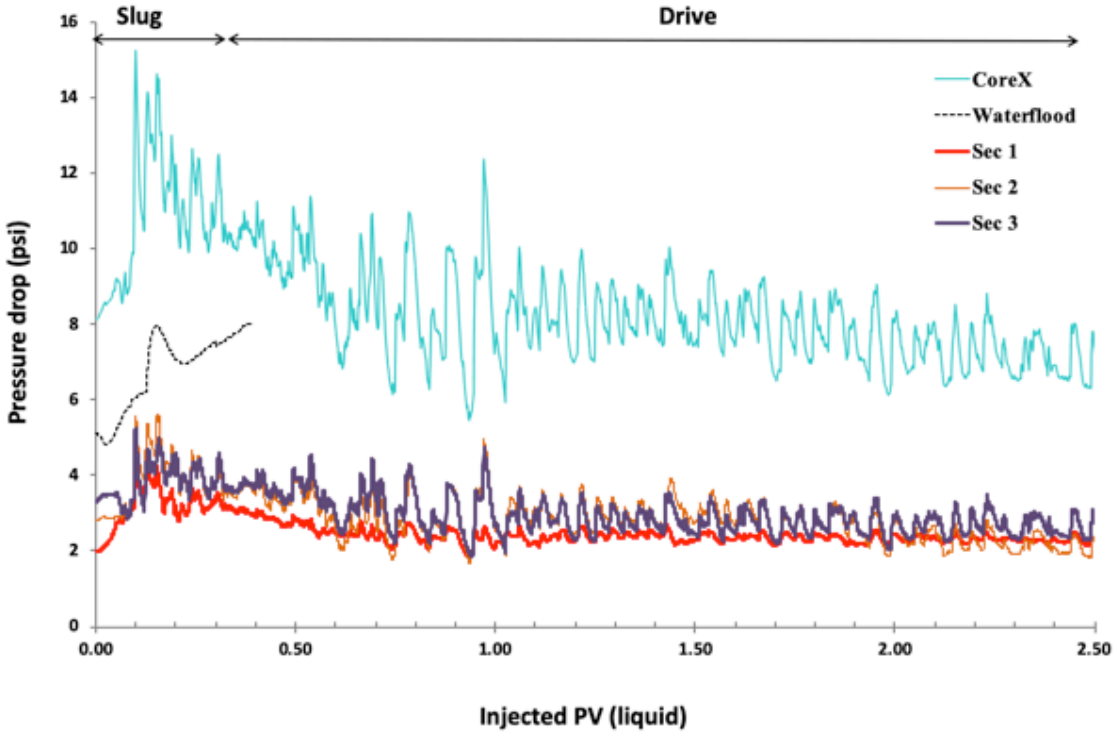

Figure 4.23: LTG injection pressure drop profile compared to waterflood of coreflood 4.

Along with the apparent viscosity data (Figure 4.24), this indicates the presence of foam and the formation of an oil bank.

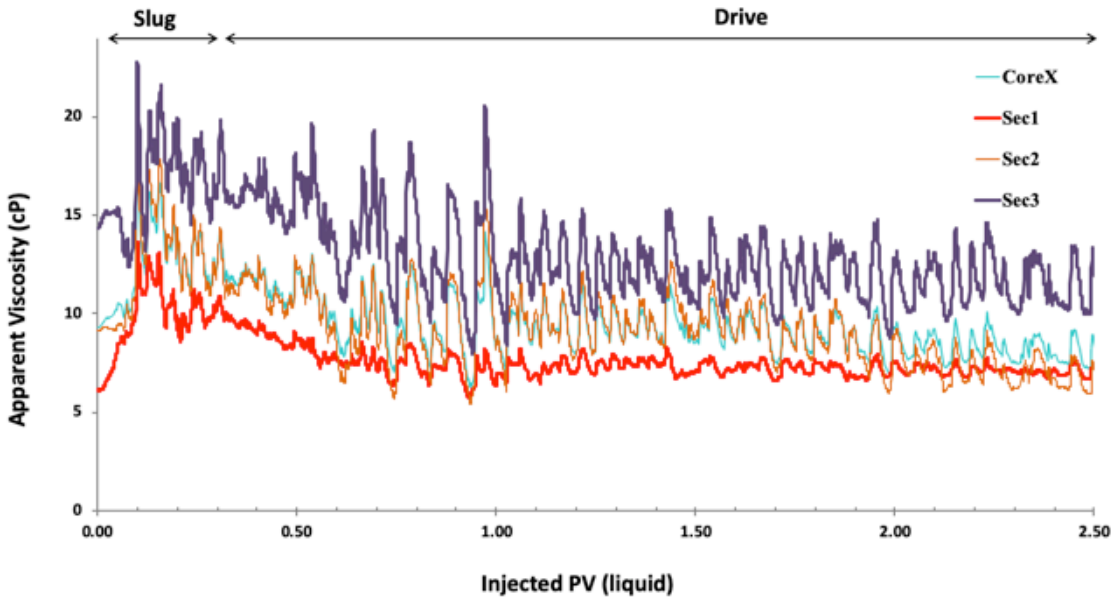

Figure 4.24: Apparent viscosity profile of coreflood 4 LTG injection.

However, the salinity data in Figure 4.25 reveals that it is very likely that solubilization from Type III microemulsion did not occur, since the Type III window occurs at much lower salinity, as shown.

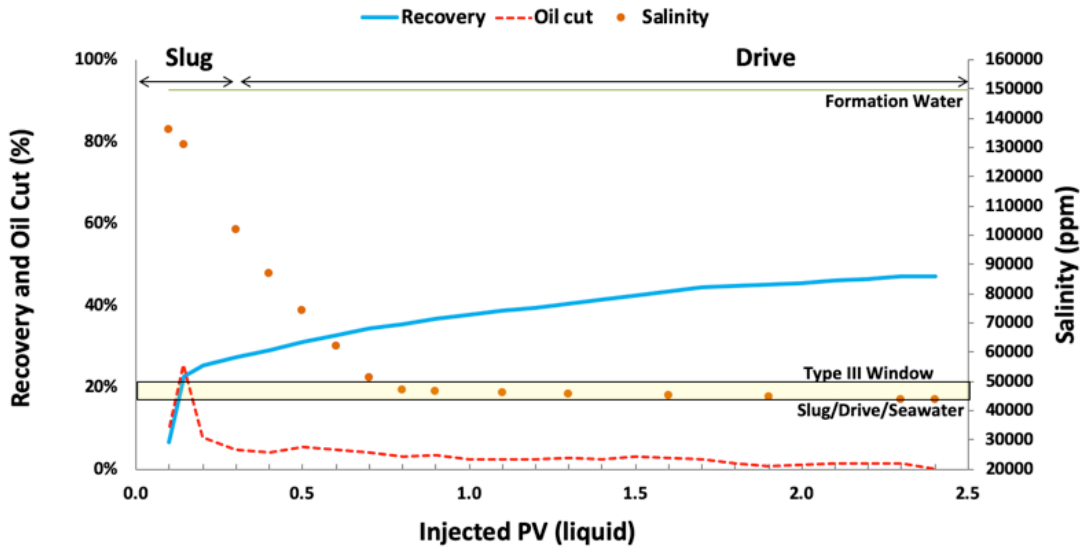

Figure 4.25: continued next page.

Figure 4.25: Salinity, oil cut, and recovery profile of coreflood 4 LTG injection with the Type III region of the Low Salinity formulation shown in yellow box.

The pressure drop profile with oil cut, oil recovery, and waterflood once again shows the pressure spike at the time of highest oil recovery. As seen in the other corefloods, the oil breakthrough occurs at approximately 0.15 liquid pore volumes injected, which is exactly half of the 0.3 liquid pore volume surfactant slug. The oil cut at the breakthrough point is higher than the other corefloods. This would not necessarily be expected when comparing the performance with the better performing corefloods 1 and 3. This could be simply due to the timing of the effluent vials switching in the effluent collector, which only has a certain degree of resolution due to the relatively large vial sizes of 0.1 liquid pore volumes injected per vial.

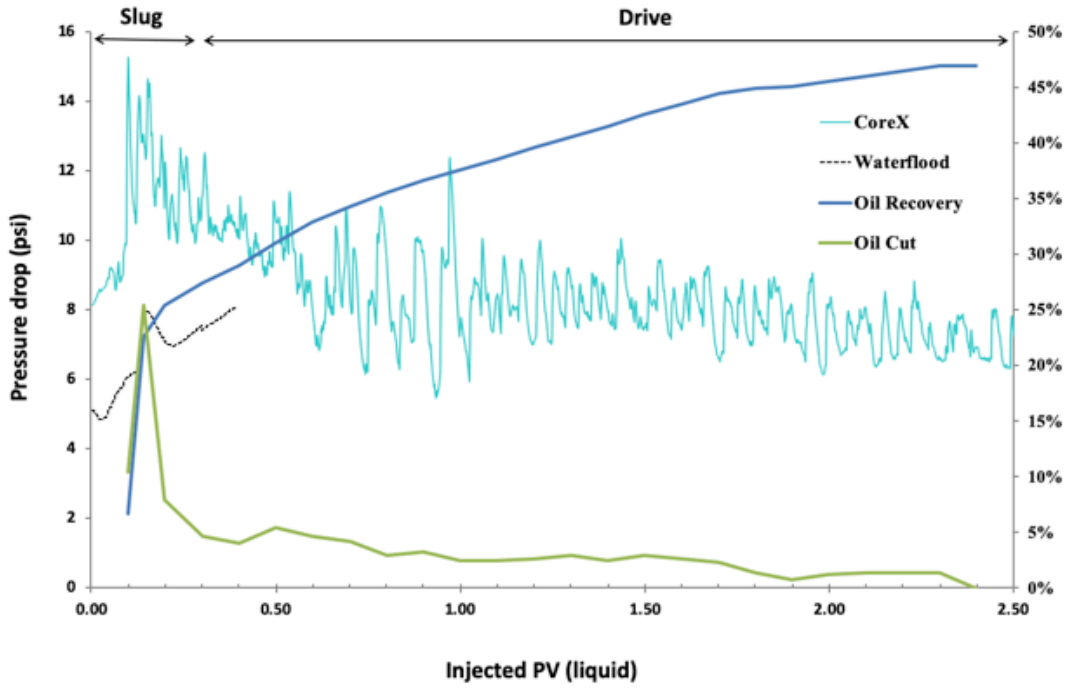

Figure 4.26: continued next page.

Figure 4.26: Core-scale LTG injection pressure drop profile compared to oil cut, oil recovery, and waterflood for coreflood 4.

Although not nearly as successful as coreflood 3, this flood still shows a positive effect of the waterflood pre-flush. This scenario, as discussed Chapter 2.5., would be where the pre-flush size is pre-determined and the optimum salinity could be altered. This coreflood is intended to show the performance of the Low Salinity formulation in contrast with the performance of the High Salinity formulation under the same conditions and similar pre-flush size.

4.2.5. Coreflood 5

Finally, a coreflood was completed with the High Salinity formulation present in the LTG injection after a pre-flush of 0.4 pore volume formation water waterflood followed by 0.2 pore volume of seawater waterflood. As previously discussed, most of the mobile oil is produced by 0.4 – 0.5 pore volume of waterflood. The hypothesis being that the 0.4 pore volume of formation water would displace most of the mobile oil, and the 0.2 pore volume pre-flush of seawater would alter the salinity effectively. The goal was to achieve similar Type III behavior on a coreflood with immature salinity mixing, as achieved in coreflood 3 by the approximately 0.433 pore volume of seawater injected. This coreflood was completed in order to observe the effect of the salinity mixing in the absence of the mobile oil.

The waterflood pressure drop profile is seen in Figure 4.27. The pressure drop profile, once again, begins to plateau at the 0.4 pore volume injected mark, with the section 3 pressure drop levelling off and even beginning to decrease. The oil saturation at the end

of waterflood, S_{orw} is 27%, with the very low oil cut indicating that the mobile oil present in the formation was produced by this duration of waterflood.

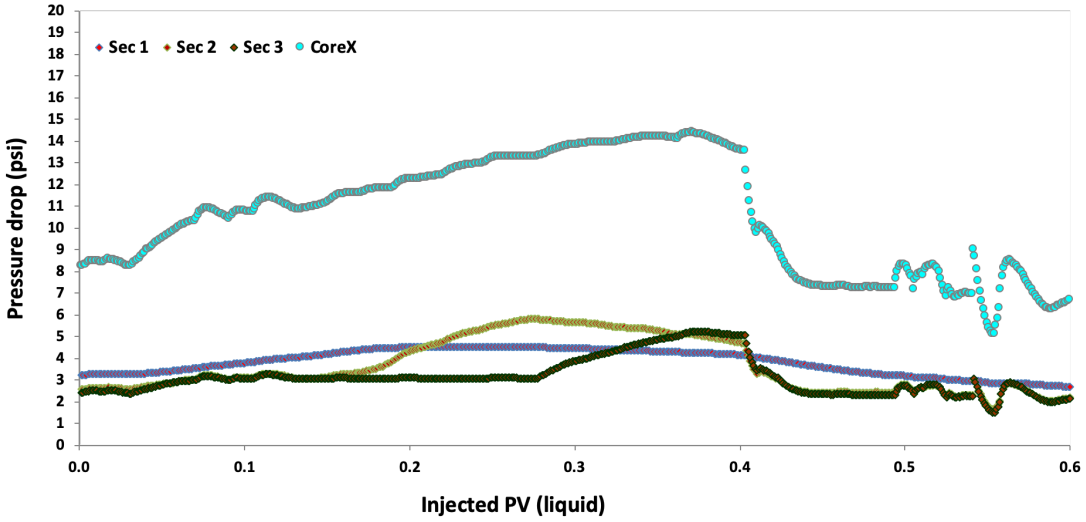

Figure 4.27: Pressure drop profile of coreflood 5 waterflood of 0.4 pore volumes of formation water and additional 0.2 pore volumes of seawater.

The waterflood showed such steep decline at the 0.4 pore volume injected mark due to the back pressure regulators slipping and releasing fluid while switching between formation brine and seawater waterfloods. The absolute pressure data supports this and is shown below, along with the waterflood profiles of all 5 corefloods for comparison. The absolute pressure data shows a disturbance at 0.4 pore volume injected, which is representative of a back pressure regulator slipping and releasing liquid during absence of flow. There should be much less of a disturbance due to the incompressible nature of the system, as no gas has been injected at this point of the coreflood experiment. However, the waterflood profile still follows the same trend of pressure drop decreasing after most mobile oil produced, which it was in this coreflood by 0.4 pore volume. This is shown by

a decline in pressure drop just before 0.4 pore volume injected and the brine switch occurring. The pressure drop profile trend on the plateau and decrease is compressed and occurs more quickly due to the back pressure regulator release.

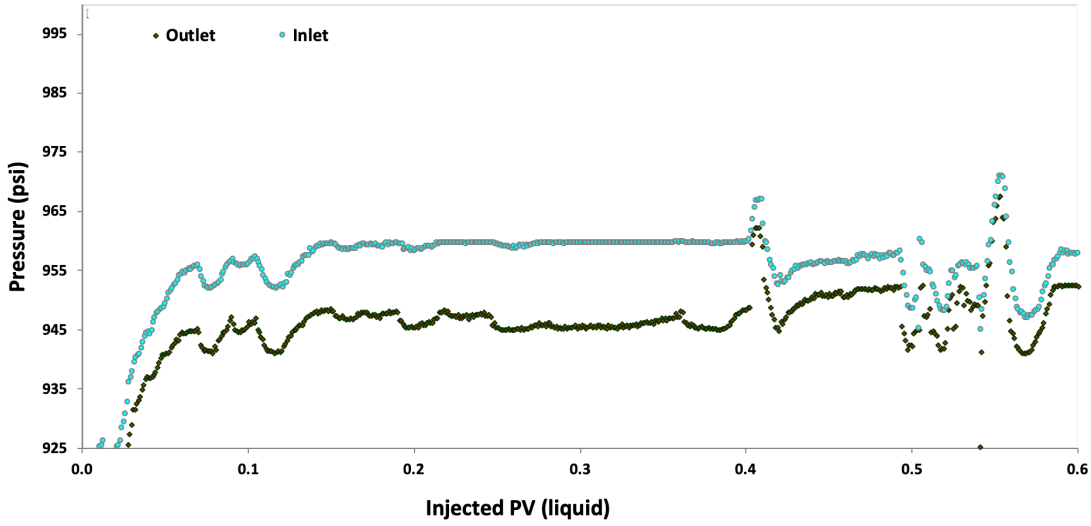

Figure 4.28: Absolute pressure profile of coreflood 5 waterflood of 0.4 pore volumes of formation water and additional 0.2 pore volumes of seawater.

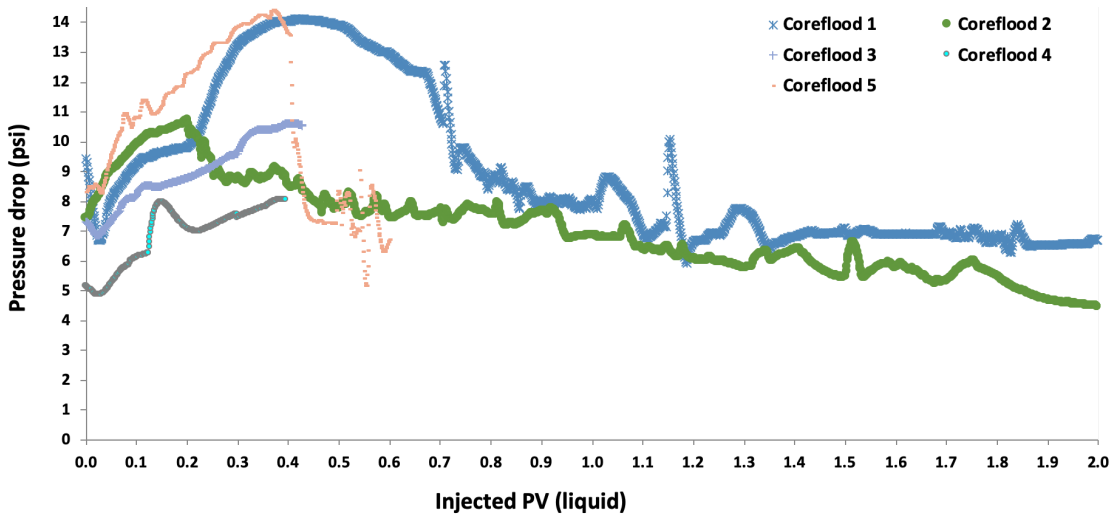

Figure 4.29: Pressure drop profile of waterflood from each coreflood experiment.

Although the waterflood pressure drop profile is not as gradually declining as the other corefloods, when compared to the LTG pressure drop profile, the peak value of approximately 14 psi can still be considered. The LTG pressure drop only achieved a pressure drop as high as the waterflood at nearly 0.5 liquid pore volume injected. This is a function of the waterflood's decrease in pressure drop in late time, and not a function of any LTG increase in pressure drop. The pressure drop profile of the LTG process indicates that little to no oil bank was formed due to foam. The presence of foam is also unlikely, which will be discussed further in the coreflood 5 salinity portion. The lack of obvious sectional pressure drop increase also supports this.

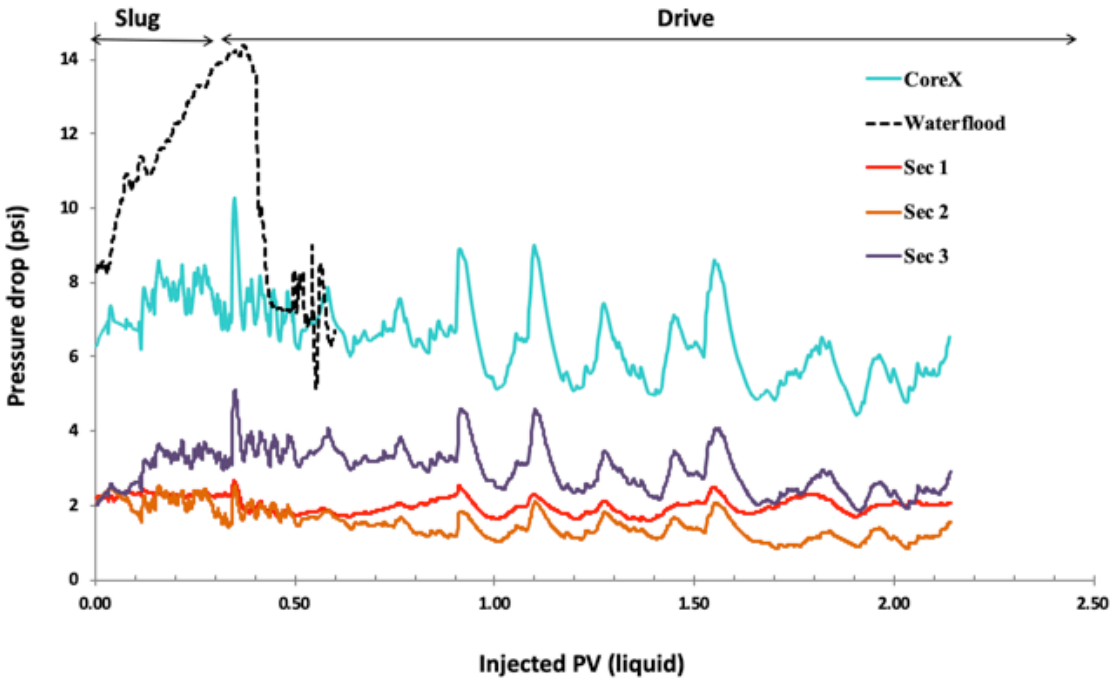

Figure 4.30: LTG injection pressure drop profile compared to waterflood of coreflood 5.

The apparent viscosity shows sectional values with little increase, again likely due to the lack of stable foam reducing the relative mobility of the injected fluids and creating resistance to flow.

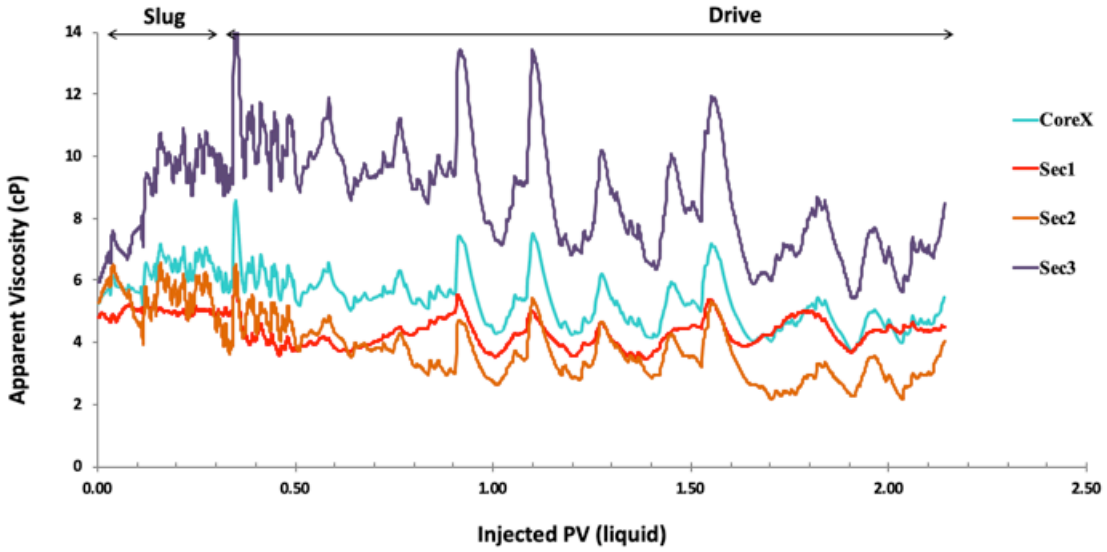

Figure 4.31: Apparent viscosity profile of coreflood 5 LTG injection.

The oil recovery profile alongside the oil cut and pressure drop profiles again show oil breakthrough at the 0.15 liquid pore volume injected mark. The recovery of this coreflood only reached approximately 35%, which is appropriate for the lack of foam formation due to the high core entry salinity for the slug formation from the inadequate pre-flush of 0.2 pore volume of seawater.

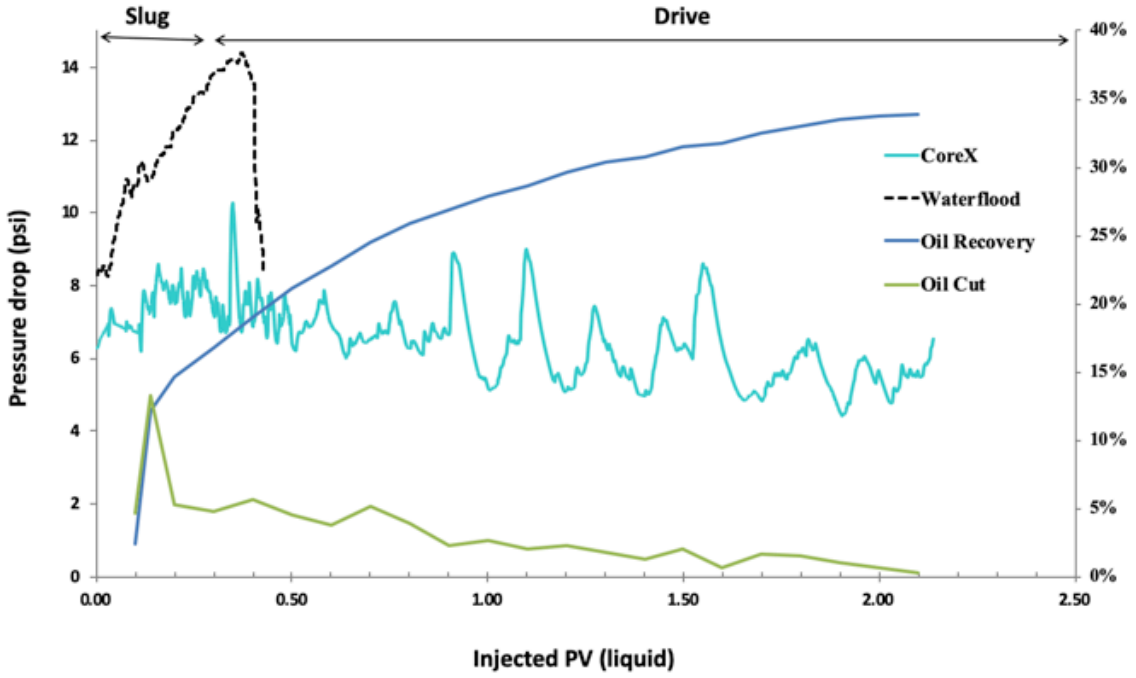

Figure 4.32: Core-scale LTG injection pressure drop profile compared to oil cut, oil recovery, and waterflood for coreflood 5.

The effluent salinity in Figure 4.33 shows that during the period of highest oil recovery, the salinity was above the Type III region of the injected chemical. With that result, this coreflood performance was suboptimal. The degree of mixing achieved from 0.4 pore volume formation water and 0.2 pore volume seawater waterflood injected between the remaining formation water and the waterflood prior to LTG was not as impactful as expected. The "pre-flush" of 0.2 pore volume seawater waterflood, even in the absence of mobile oil, was not enough to properly condition the core for the High Salinity formulation to be successful. 0.2 pore volume of seawater waterflood injected is below the critical pre-flush required to alter the salinity substantially enough for the Type III salinity of the formulation. The foam likely coalesced quickly due to the high salinity, Type II environment above the aqueous stability, and did not mobilize much oil to form a

strong oil bank, given by the pressure drop lower than waterflood and lack of sectional pressure drop increase typically seen in LTG corefloods.

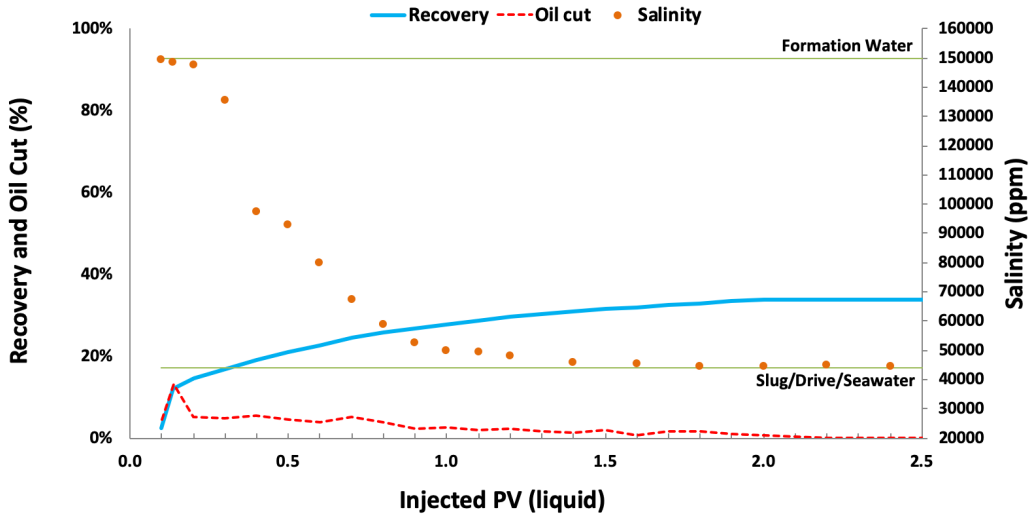

Figure 4.33: Salinity, oil cut, and recovery profile of coreflood 5 LTG injection with the Type III region of the Low Salinity formulation shown in yellow box.

4.2.6. Coreflood Summary

The summary of the five corefloods experiments and the calculated results can be found in Table 4.1.

CF	Waterflood Type	LTG Formula	S_{oi}	S_{orw}	EOR Recovery
1	Mature – SW	Low Salinity	63%	22%	75%
2	Mature – FW	Low Salinity	53%	22%	35%
3	0.4PV – SW	High Salinity	56%	18%	81%
4	0.4PV – SW	Low Salinity	60%	28%	47%
5	0.4PV–FW → 0.2PV–SW	High Salinity	61%	27%	34%

Table 4.1: continued next page.

Table 4.1: Experimental and calculated results for corefloods 1 through 5.

4.3. Pressure Drop

The pressure drop profiles of all five corefloods are shown in Figure 4.34. The three highest peak pressure drops are corefloods 1, 4, and 3, in order of highest to lowest pressure drop attained. Coreflood 1 has a very large pressure drop compared to the other corefloods. This is expected given the entire LTG injection occurring at optimum Type III salinity, creating a large oil bank from Type III microemulsion, followed by the surfactant foam front.

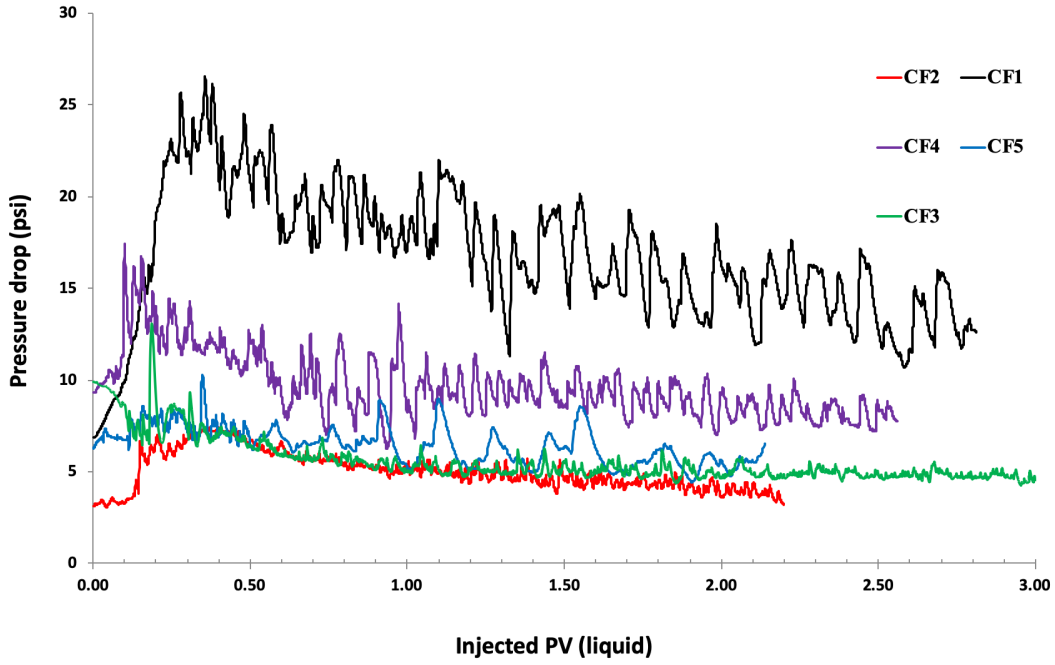

Figure 4.34: LTG injection pressure drop profiles of all 5 corefloods.

4.4. Apparent Viscosity

Coreflood 1, along with the highest pressure drop also has the highest apparent viscosity values. This is again, likely due to the strong oil and surfactant bank attained from the Type III salinity environment. This environment was conducive in generating the greatest resistance to flow and lowest relative mobility of all the corefloods. Each coreflood has a weighted average apparent viscosity above the viscosity of the oil, 5.25cP. This shows that the displacing phases were capable of mobilizing residual oil and displacing it through the core, due to higher capillary number during LTG from increased viscous effects.

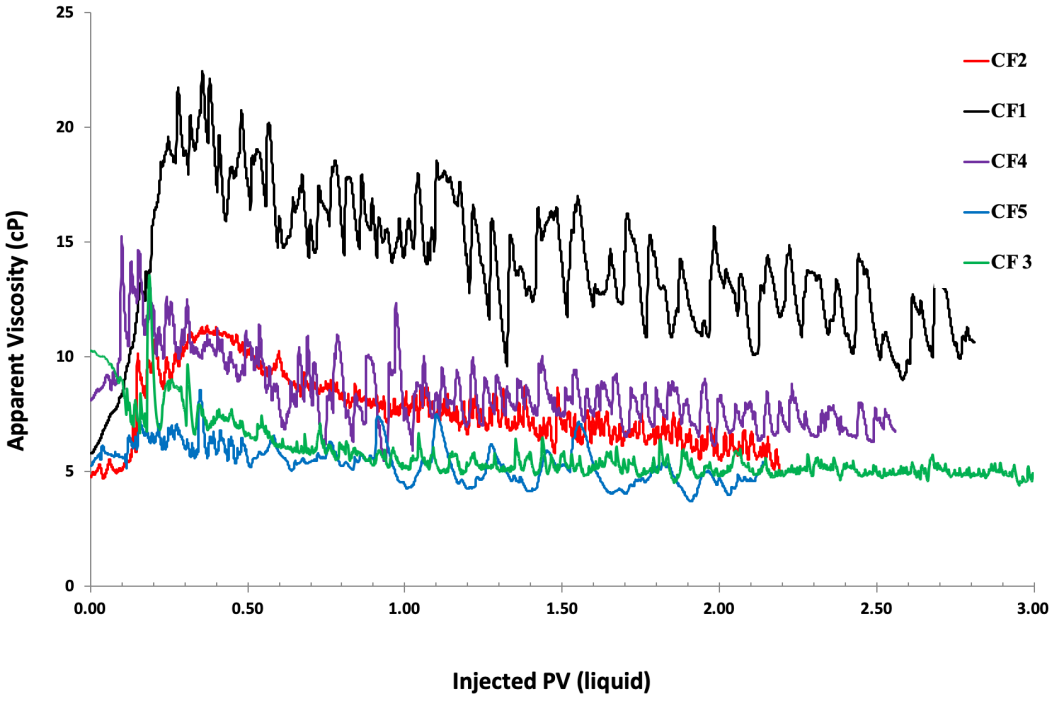

Figure 4.35: Apparent viscosity profiles of all 5 corefloods.

4.5. Oil Recovery

Figure 4.36 shows the recovery profiles of each coreflood. Relatively equal increases in recovery are shown in corefloods 1, 3, and 4. However, the coreflood that maintained this slope of increasing recovery is coreflood 3, the highest performing coreflood. One of the two worst performing corefloods, coreflood 2 has the most gradual increase in oil recovery, but maintains slight oil production longer than coreflood 5. The slight oil recovery over long durations after the initial oil recovery spike is due to the increased capillary number during the LTG process from interfacial tension reduction due to microemulsion or increased viscous effects due to foam.

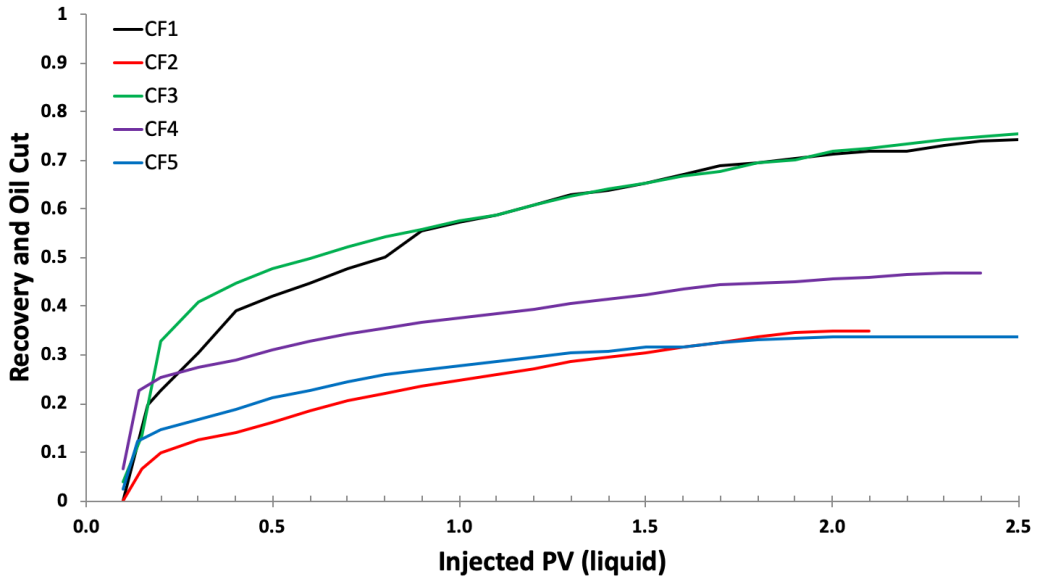

Figure 4.36: Oil recovery profiles of all 5 corefloods.

4.6. Oil Cut

Figure 4.37 shows the oil cut profiles of each coreflood experiment. As expected, corefloods 1 and 3, the highest performing corefloods (75% and 81% EOR recovery, respectively) have two of the sharpest and broadest initial oil cut region between 0.15 and 0.5 liquid pore volumes expected. The high oil cut of coreflood 4, as previously discussed in the coreflood 4 section, is likely due to the timing of the effluent collector, and should be considered an artifact of the experimental setup, given its relatively low recovery and performance. Coreflood 2 achieved the lowest peak oil cut, which corresponds to the low recovery of 35%. The oil cut behavior is in line with the ultimate recoveries of each coreflood.

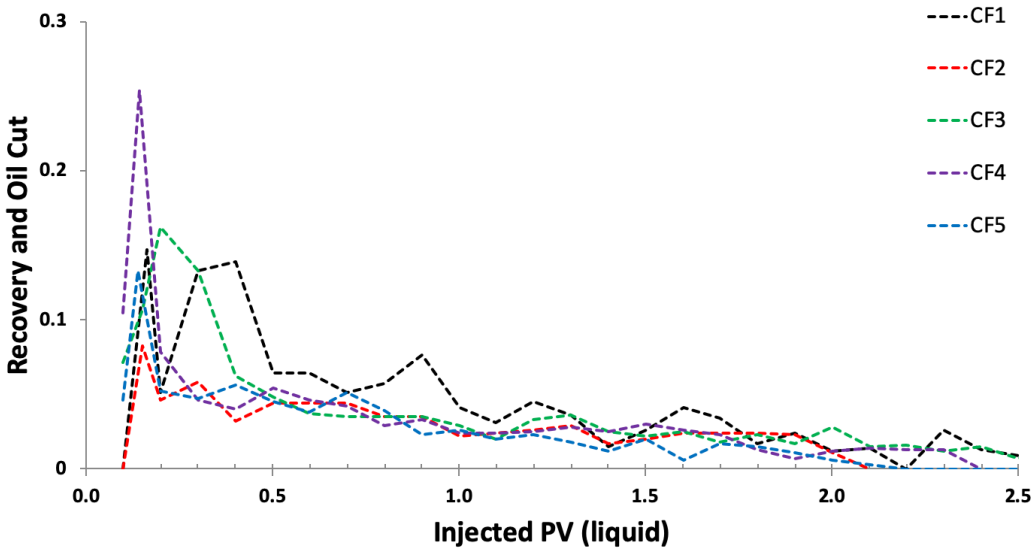

Figure 4.37: Oil cut profiles of all 5 corefloods.

4.7. Effluent Salinity

For LTG flooding, the effluent salinity is a highly important measurement for the evaluation and interpretation of the mobility control present in the coreflood. The salinity data during LTG for all corefloods is shown in Figure 4.38. Coreflood 1 has no LTG salinity data because the only salinity change occurring in that flood is through the mature waterflood from formation water down to seawater salinity. There exist two separate flow behaviors in these LTG floods, where dispersion is decreased and where dispersion is increased. Both can be identified by the manner in which the salinity decreases. A sharp decrease indicates reduced dispersion, and a sharper shock front propagation. Szlendak (2012) describes this phenomena, showing that an increased shock strength, signified by the sharp salinity decrease, is "indicative of improved displacement of fluids during production of reservoir brine and oil bank." Whereas a gradual decrease indicates an unfavorable environment where injected fluids finger through the formation, with increased dispersion between the slug solution and resident formation brine. As the gas saturation reaches the ultimate value, Das (2020) states that due to the gas injected, the volume for mixing is reduced due to foam in the mixing zone between the resident brine and the surfactant slug/drive solution. In these cases, Lake (1989) shows that mechanical dispersion will also increase, as the interstitial fluid velocity increases. This is due to the reduction of pore volume available to the injected liquid being reduced, while the injected rate remains constant.

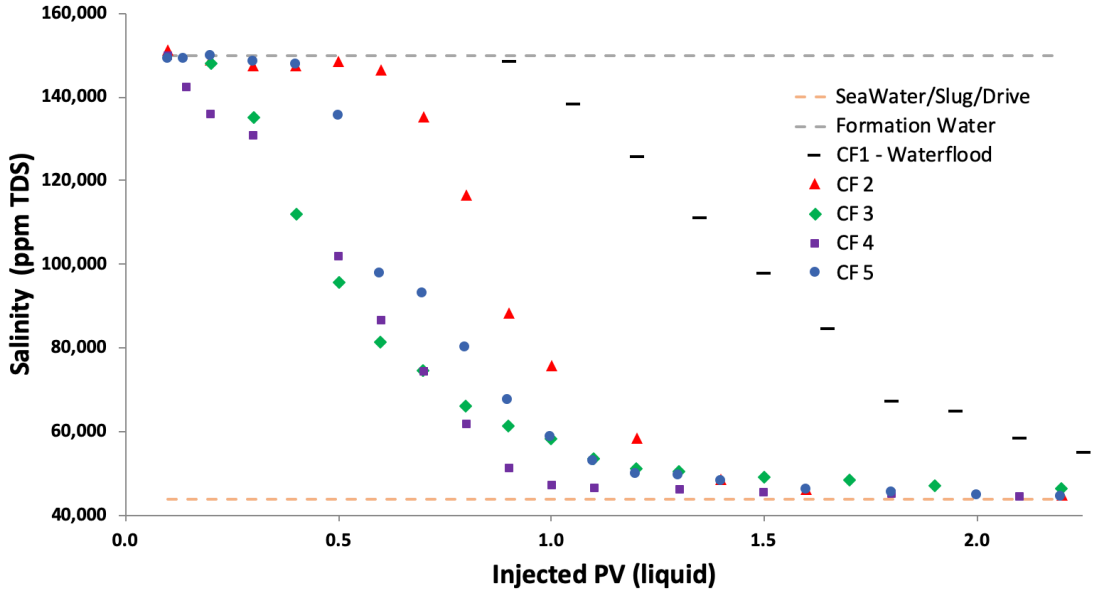

Figure 4.38: Effluent salinity profiles of all 5 corefloods.

The starting point of the salinity decrease for each coreflood occurs at a different amount of injected pore volumes due to the varied waterflood durations of each coreflood. To recap, fully mature waterfloods for corefloods 1 (seawater) and 2 (formation water), 0.4 pore volume of seawater waterflood pre-flush for corefloods 3 and 4, and a total waterflood of 0.6 pore volume for coreflood 5, comprised of 0.4 pore volume formation water and 0.2 pore volume seawater. To allow for better interpretation of the salinity data, Figure 4.39 depicts the salinity data of the corefloods with the initial decrease in salinity for each beginning at the same datum.

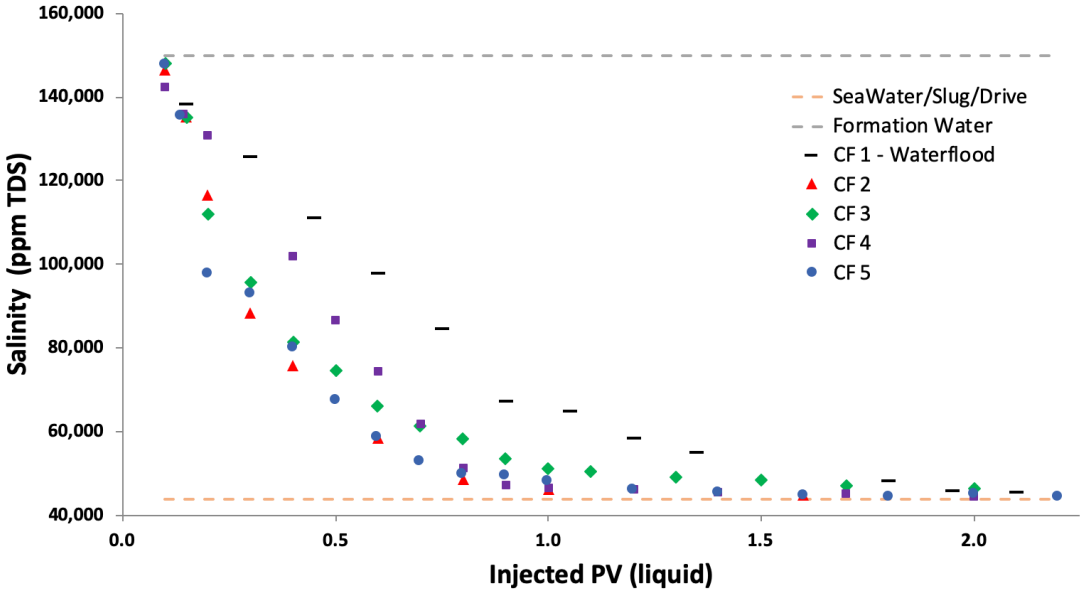

Figure 4.39: Effluent salinity profiles of all 5 corefloods beginning at the same datum.

Corefloods 2, 3, and 5 appear to have the sharpest initial declines in salinity, showing that they achieved the best mobility control and propagation of a sharp shock front. Coreflood 4 has a much more gradual decrease in salinity, indicative of less mobility control, and increased dispersion than the other three corefloods mentioned above. This behavior is also observed in the waterflood salinity data of coreflood 1.

Each coreflood exhibits the slowing of the salinity change at varying points along their progression from formation water salinity to seawater salinity. In all floods this occurs after the high oil cut region and majority of oil has been produced. This means that the injected fluids are beginning to finger through the core more as there exist no higher viscosity fluids (microemulsion and oil) left to produce. Any remaining resident formation brine is not produced out of the formation as effectively, and it remains in the formation for longer, as injected fluids bypass.

CHAPTER 5: CONCLUSION AND RECOMMENDATIONS

5.1. Conclusion

The use of Low and High Salinity formulations in tandem with varied waterflood liquids and injection amounts was an effective method of determining the presence of a critical waterflood pre-flush, as outlined in the methodology. Not only was the duality of waterflood maturity in oil saturation and salinity mixing identified, but the various effects of salinity mixing was analyzed, as oil saturation was held relatively constant. The salinity mixing of the critical pre-flush between the resident and injected brines allows a favorable, less harsh salinity environment for LTG injection. The critical pre-flush for these experimental conditions was identified to be between 0.2 and 0.433 pore volumes of waterflood, for the High Salinity formulation. The existence of a correlation between waterflood maturity and the appropriate optimums salinity of a surfactant formulation for EOR is evident.

This novel idea of waterflood critical pre-flush could have a lasting and profound effect on offshore operating areas with an abundant source of seawater, with similar surfactant capabilities available. Operations with the availability of lower salinity freshwater can also apply the findings of this work. Not only does the critical pre-flush produce oil to the formation's residual value, but it also better prepares the formation for surfactant injection, in this case, LTG injection. The advantage of reducing waterflood duration from multiple pore volumes to a fraction of that will also greatly improve the economic viability of a particular project. This correlation established could have a profound effect when taking into account waterflood and chemical EOR planning.

5.2. Recommendations

Based on the results of this work, the author would like to make the following recommendations that will further improve the understanding of the critical pre-flush regarding LTG technology:

- Continued LTG experiments of varying waterflood pre-flush sizes will allow for more "data points" and further resolution of the correlation between the waterflood maturity and the appropriate optimum salinity.
    - This will allow one to generate a critical waterflood pre-flush size depending on the appropriate optimum salinity of a formulation, which may depend on surfactant capability or availability.
- Investigation of Surfactant-Alternating-Gas (SAG) injection as a possible technique that can further scale this work for applicability to the field.

References

Blaker, T., Aarra, M. G., Skauge, A., Rasmussen, L., Celius, H. K., Martinsen, H. A., & Vassenden, F. (2002, August 1). Foam for Gas Mobility Control in the Snorre Field: The FAWAG Project. Society of Petroleum Engineers. doi:10.2118/78824-PA

Bikerman, J.J.: Foams, Springer Verlag, New York (1973)

Bond, D. C. and Holbrook, C. C.: "Gas Drive Oil Recovery Process", U.S. Patent No. 2,866,507 (December 1958)

Chambers, K. T. M.S. Thesis, University of California, Berkeley, CA, 1990.

Chambers, K.T. and Radke, C.J., Interfacial Phenomena in Petroleum Recovery, Marcel Dekker: New York, 1991.

Conn, C.A., Ma, K., Hirasaki, G.J. *et al*. 2014. Visualizing Oil Displacement with Foam in a Microfluidic Device with Permeability Contrast. Lab Chip 14 (20): 3968–3977. https://doi.org/10.1039/c4lc00620h.

Das, A., Nguyen, N., Alkindi, A., Farajzadeh, R., Azri, N., Southwick, J., Vincent-Bonnieu, S., Nguyen, Q. P. (2016, March 21). Low Tension Gas Process in High Salinity and Low Permeability Reservoirs. Society of Petroleum Engineers. doi:10.2118/179839-MS

Das, A., Nguyen, N., Nguyen, Q.P., Low tension gas flooding for secondary oil recovery in low-permeability, high-salinity reservoirs, Fuel, Volume 264, 2020, 116601, ISSN 0016-2361, https://doi.org/10.1016/j.fuel.2019.116601.

Green, D.W. and Willhite, G.P., Enhanced Oil Recovery, SPE, 1998.

Hirasaki, G. J., Miller, C. A., Szafranski, R., Tanzil, D., Lawson, J. B., Meinardus, H., Jin, M., Londergan, J.T., Jackson, R.E., Pope, G.A., Wade, W. H. (1997, January 1). Field Demonstration of the Surfactant/Foam Process for Aquifer Remediation. Society of Petroleum Engineers. doi:10.2118/39292-MS

Huh, C. "Interfacial Tensions and Solubilizing Ability of a Microemulsion Phase That Coexists with Oil and Brine," Journal of Colloid and Interface Science (1979), 71 (2): 408-426

Islam, M. R., and Farouq Ali, S. M.: "Numerical Simulation of Foam Flow in Porous Media," JCPT (August 1990), 29, No 4,47-51

Jiménez, A. I., Radke, C. J.in Oil-Field Chemistry: Enhanced Recovery and Production Stimulation; Borchardt, J. K.; Yen, T. F., Eds.; ACS Symposium Series 396; American Chemical Society: Washington, DC, (1989) 460-479.

Jong, S., Nguyen, N. M., Eberle, C. M., Nghiem, L. X., & Nguyen, Q. P. (2016, April 11). Low Tension Gas Flooding as a Novel EOR Method: An Experimental and

Theoretical Investigation. Society of Petroleum Engineers. doi:10.2118/179559-MS

Kovscek AR and CJ Radke. 1994. "Fundamentals of From Transport in Porous Media." Chapter 3 in Schramm, L.L., Foam: Fundamentals and Applications in the Petroleum Industry, Washington, D.C. American Chemical Society

Lake, L.W. 1989. Enhanced Oil Recovery. Prentice-Hall, Upper Saddle River, NJ.

Lawson, J. B., & Reisberg, J. (1980, January 1). Alternate Slugs Of Gas And Dilute Surfactant For Mobility Control During Chemical Flooding. Society of Petroleum Engineers. doi:10.2118/8839-MS

Marfoe, C. H., and Kazemi, H.: "Numerical Simulation of Foam Flow in Porous Media," paper SPE 16790 presented at the 1987 Annual Technical Conference and Exhibition of the SPE, Dallas, TX 27-30.

Mast, R. F. (1972, January 1). Microscopic Behavior of Foam in Porous Media. Society of Petroleum Engineers. doi:10.2118/3997-MS

Nguyen, Q. P., Alexandrov, A. V., Zitha, P. L., & Currie, P. K. (2000, January 1). Experimental and Modeling Studies on Foam in Porous Media: A Review. Society of Petroleum Engineers. doi:10.2118/58799-MS

Nguyen, Q. P., Currie, P. K., & Zitha, P. L. J. (2005, March 1). Effect of Crossflow on Foam-Induced Diversion in Layered Formations. Society of Petroleum Engineers. doi:10.2118/82270-PA

Nguyen, N., Ren, G., Mateen, K., Cordelier, P. R., Morel, D. C., & Nguyen, Q. P. (2015, August 11). Low-Tension Gas (LTG) Injection Strategy in High Salinity and High Temperature Sandstone Reservoirs. Society of Petroleum Engineers. doi:10.2118/174690-MS

Owete, O. S., & Brigham, W. E. (1987, August 1). Flow Behavior of Foam: A Porous Micromodel Study. Society of Petroleum Engineers. doi:10.2118/11349-PA

Prieditis, J. Ph.D. Thesis, University of Houston, Houston, TX, 1988.

Ransohoff, T. C., and Radke, C. J. "Mechanisms of Foam Generation in Glass-bead Packs," SPE Reservoir Evaluation & Engineering (May 1988), 3 (2): 573-585

Sanders, A. W., Jones, R. M., Linroth, M. A., & Nguyen, Q. P. (2012, January 1). Implementation of a CO2 Foam Pilot Study in the SACROC Field: Performance Evaluation. Society of Petroleum Engineers. doi:10.2118/160016-MS

Schramm, L.L. 1994. Foams: Fundamentals & Applications in the Petroleum Industry, ACS Advances in Chemistry Series 242, American Chemical Society, Washington, DC.

Sheng, J.J., Status of surfactant EOR technology, Petroleum, Volume 1, Issue 2, 2015, Pages 97-105, ISSN 2405-6561, https://doi.org/10.1016/j.petlm.2015.07.003.

Szlendak, S., Nguyen, N., & Nguyen, Q. P. (2012, January 1). Successful Test of Low-Tension-Gas (LTG) Flooding for Tertiary Oil Recovery in Tight Formations (<10mD to Gas). Society of Petroleum Engineers. doi:10.2118/159841-MS

Veeningen, D., Zitha, P. L. J., & van Kruijsdijk, C. P. J. W. (1997, January 1). Understanding Foam Flow Physics: The Role of Permeability. Society of Petroleum Engineers. doi:10.2118/38197-MS

Wang, D., Cheng, J., Yang, Z., Qun, L., Wu, W., & Yu, H. (2001, January 1). Successful Field Test of the First Ultra-Low Interfacial Tension Foam Flood. Society of Petroleum Engineers. doi:10.2118/72147-MS

Weaire, D. and Hutzler, S. "A Review of Foam Drainage," Advances in Chemical Physics (1997), 102: 315.